# Synthesis, Structural Characterization, and Magnetic Properties of a New Series of Coordination Polymers: Importance of Steric Hindrance at the Coordination Sphere

Paulami Manna, Bharat Kumar Tripuramallu, and Samar K. Das*

School of Chemistry, University of Hyderabad, P.O. Central University, Hyderabad, 500046, India

S Supporting Information

ABSTRACT: Six cobalt(II) containing coordination polymers {Co(hfipbb)-(L1)$_{0.5}$}$_n$ (**1**), {Co(hfipbb)(L2)$_{0.5}$}$_n$ (**2**), {Co(oba)(L1)$_{0.5}$}$_n$ (**3**), {Co(oba)-(L2)}$_n$·nH$_2$O (**4**), {Co(1,2-pda)(L1)$_{0.5}$}$_n$ (**5**), and [Co(1,2-pda)(L2)-(H$_2$O)]$_n$·nH$_2$O (**6**), that are formed from two positional isomeric bis(pyridyl) ligands with a long flexible spacer 1,4-bis(2-pyridylaminomethyl)benzene (**L1**) and 1,4-bis(3-pyridylaminomethyl)benzene (**L2**) and three different bent carboxylic acids 4,4′-(hexa-fluoroisopropylidene)bis-(benzoicacid) (H$_2$hfipbb), 4,4′-oxyben-zoic acid (H$_2$oba), and 1,2-phenylenediaceticacid (1,2-H$_2$pda), have been synthesized under hydrothermal conditions. Compounds **1−6** are characterized by single crystal X-ray diffraction analysis, IR spectroscopy, and thermogravimetric (TG) and elemental analysis. In the crystal structures of compounds **1**, **3**, and **5**, two-dimensional (2D) metal-carboxylic acid layers, composed of dicobalt tetracarboxylate paddle-wheel clusters, are formed whereby these layers are pillared by the secondary ligand **L1** in a typical *trans−trans−trans* conformation to result in a three-dimensional (3D) layered-pillared structure. However, in the crystals of compounds **2**, **4**, and **6** with secondary ligand **L2**, it does not favor the formation of paddle-wheels resulting in three completely different coordination polymers. The geometry of the carboxylic acid influences the formation of 2D metal acid layers in the compounds **1**, **3**, and **5** to form interpenetrated helical double layers to single layers. In compound **2**, the secondary ligand **L2** diagonally connects the 3D metal acid framework in a regular *trans−trans−trans* conformation. In compound **4**, the ligand **L2** exists in *cis−cis−trans* conformation to form [Co$_2$L2$_2$] loops (metallo-macrocycles) which are connected by the oba$^{2−}$ ligand to form polyrotaxane-like 2D polymers. In compound **6**, ligand **L2** exists in an unusual *cis−trans−cis* conformation to allow the pda$^{2−}$ in a rare cis conformation to form one-dimensional (1D) ladders. The conformations of the pyridyl ligands **L1** and **L2** have been explained based on the torsion angle measurement. The steric hindrance created by the isomeric flexible pyridyl ligands at the metal coordination sphere plays an important role in the modulation of the conformation of the secondary ligand that drives the self-assembly of the coordination polymers. Finally, temperature-dependent magnetic susceptibility studies for the compounds **1−5** have been described.
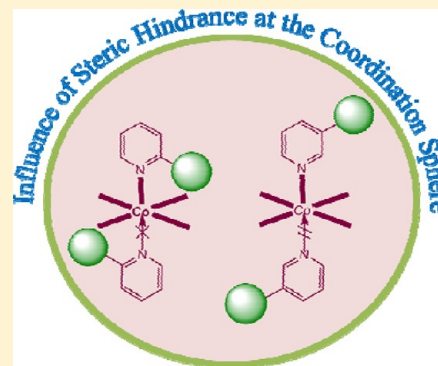
INTRODUCTION

The design and assembly of metal−organic frameworks (MOFs) have become a focus of a great deal of interest in recent years due to not only their undisputed structural beauty and entangled architectures but also potential application in areas such as catalysis, gas storage, separation, magnetism, luminescence, nonlinear optics, sensing, and so on.[1] The choice of ligand plays an influential role in designing the target polymers depending on the geometry and properties, such as, the spacing between the coordination sites, orientation of the donor atoms, flexibility or rigidity of the ligand, and the various coordination modes of the ligand. Construction of the coordination polymers by using the mixed ligand often leads to versatile topologies with intriguing functional properties and porous MOFs.[2] To date, a mixture of carboxylic acids and N-containing auxiliary ligands is successfully used to obtain a range of polymeric structures with interesting properties.[3] The introduction of the N-containing ligands like amines, imines, azoles, etc. allow us to tune the dimensionality of metal

polycarboxylate architectures with desired topologies and also to study the mechanism of the self-assembly processes. Coordination architectures containing highly connected metal cluster nodes are of current interest in exploring the magnetic properties through the OCO bridge. Dinuclear paddle-wheel, a simple building unit (SBU) used as a node in constructing the coordination polymers, is highly explored with and without using N-containing ligands (Scheme 1).[4] The availability of the two apical coordination sites on the paddle-wheel allows us to introduce the secondary ligand, which not only results in extending the dimensionality of the paddle-wheel but also brings an enormous structural change in the geometry of paddle-wheel.
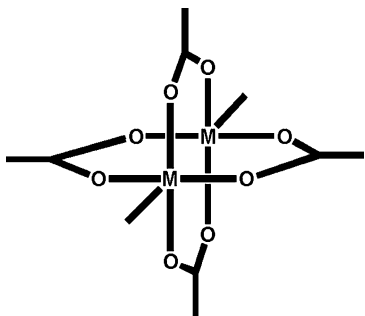
The geometry of the secondary ligands used may be rigid, bent, or flexible, which has a direct consequence on the

Scheme 1. Schematic Representation of a Paddle-Wheel

topology of the resulting structure attained. The coordination networks based on rigid bridging ligands such as 4,4′-bipyridine, pyrazine, phenazine, quinoxaline, 4-pyridyl tetrazole, 1,2-dpe, etc. are extensively studied due to their regular coordination modes.[5] In contrast, flexible ligands are less explored in the rational design of coordination polymers, because it is more difficult to predict the final architectures owing to their greater number of degrees of freedom and hence few conformational restraints.[6] Cao et al. reported a series of coordination polymers based on the flexible ligands and used these compounds as functional materials for potential applications.[7] In our previous report, we have discussed the factors affecting the conformational modulation of the flexible ligands in the self-assembly process and the effect of solvent molecules in directing the dimensionality of coordination networks from one-dimensional (1D) to three-dimensional (3D).[8]

On the basis of aforementioned considerations, we have chosen the mixed ligand system constituted by the bent carboxylic acids as primary ligands and long flexible ligands as secondary ligands to construct the coordination architectures with Co(II) metal. Numerous coordination networks containing compounds, based on the bent carboxylic acids, are reported in which most of them have interpenetrated topologies.[9] The degree of interpenetration mainly depends on the dihedral angle between the two carboxylic groups of the ligand. On the other hand, pyridine ligands with flexible spacers such as aliphatic $(-(CH_2)_n-)$,[10] thio $(-S-(CH_2)_n-S-)$,[11] Schiff base type $(-CH=N-(CH_2)_n-N=CH-)$,[12] amide $(-CONH-(CH_2)_n-CONH-)$,[13] and ether $(-C-O-(CH_2)_n-O-C-)$,[14] etc. have been widely explored as secondary ligands. The pyridine rings separated by reduced Schiff base type flexible spacer $(-CH_2-NH-(CH_2)_n-NH-CH_2-)$ are less explored in the literature. So we have chosen the ligand with the long flexible spacer $(-NH-CH_2-(C_6H_4)-CH_2-NH-)$ between the two pyridine rings, namely, 1,4-(bis(n-pyridylaminomethyl)benzene [where, $n = 2$ (**L1**); $n = 3$ (**L2**)] to study their effect on the topology of the resulting metal polycarboxylates (see Scheme 2). In the literature, these ligands were used as only primary ligands in the construction of

coordination polymers to date. Gao et al. reported a series of compounds based on these ligands with unipositive metals Cu(I) and Ag(I) and dispositive metals Zn(II), Cd(II), and Hg(II) by employing different counteranions such as NO_3^-, SO_4^{2-}, ClO_4^-, and X^- (Br$^-$, I$^-$).[15] Because of the presence of two flexible groups i.e., $-CH_2-$ and $-NH-$ groups, it tends to adopt different conformations based on the metal coordination geometries and counteranions. So far, the ligands **L1** and **L2** are not used as secondary ligands to study their conformations along with polycarboxylates in the coordination matrix. Herein, we report the six new compounds, namely, [Co(hfipbb)(**L1**)$_{0.5}$]$_n$ (**1**), [Co(hfipbb)(**L2**)$_{0.5}$]$_n$ (**2**), [Co(oba)(**L1**)$_{0.5}$]$_n$ (**3**), [Co(oba)(**L2**)]$_n$·nH$_2$O (**4**), [Co(1,2-pda)(**L1**)$_{0.5}$]$_n$ (**5**), and [Co(1,2-pda)(**L2**)(H$_2$O)]$_n$·nH$_2$O (**6**) in which **L1** and **L2** are used as secondary ligands for the first time with Co(II) metal along with the bent carboxylic acids.

To study the effect of conformational freedom of these ligands and change in the position of the ligating atoms on the bent carboxylate systems, we have chosen three different bent dicarboxylic acids H$_2$hfipbb, H$_2$oba, and H$_2$pda. The change in the position of the ligating atom in the secondary ligand alters the formation of the SBU, mainly, due to the steric hindrance created by the bulky spacer of the ligands **L1** and **L2** in the coordination sphere. We have also studied the temperature-dependent magnetic susceptibility measurements for the compounds based on the separation between the metal centers.

■ EXPERIMENTAL SECTION

Materials and Methods. All the chemicals were received as reagent grade and used without any further purification. The ligands **L1** and **L2** were prepared according to the literature procedures.[16] Elemental analyses were determined by FLASH EA series 1112 CHNS analyzer. Infrared spectra of solid samples obtained as KBr pellets on a JASCO-5300 FT-IR spectrophotometer. Thermogravimetric analyses were carried out on a STA 409 PC analyzer and corresponding masses were analyzed by QMS 403 C mass analyzer, under the flow of N$_2$ gas with a heating rate of 5 °C min^{-1}, in the temperature range of 30−1000 °C. Powder X-ray diffraction patterns were recorded on a Bruker D8-Advance diffractometer using graphite monochromated CuK$_{\alpha 1}$ (1.5406 Å) and K$_{\alpha 2}$ (1.54439 Å) radiations. The electronic absorption spectra have been recorded on a Cary 100 Bio UV−visible spectrophotometer at room temperature. Magnetic susceptibilities were measured in the temperature range 2−300 K on a Quantum Design VSM-SQUID. All the compounds were synthesized in 23 mL Teflon-lined stainless vessels (Thermocon, India).

Synthesis of {Co(hfipbb)(L1)$_{0.5}$}$_n$ (1). A mixture of CoCl$_2$·6H$_2$O (0.25 mmol, 59.5 mg), H$_2$hfipbb (0.25 mmol, 98.0 mg), and **L1** (0.25 mmol, 72.5 mg) in H$_2$O (10.0 mL) and DMF (2.0 mL) was stirred for 30 min and then the pH of the reaction mixture was adjusted to 8.50 by adding 5 M NaOH. The reaction mixture was placed in a 23 mL Teflon-lined stainless steel autoclave and was sealed and heated at 160 °C for 72 h. The autoclave was allowed to cool to room temperature for 48 h. Deep red needle crystals of compound **1** were obtained in 65.5% yield (based on Co). Anal. Calcd for C$_{26}$H$_{17}$CoF$_6$N$_2$O$_4$ (M_r = 594.34): C, 52.54%; H, 2.88%; N, 4.71%. Found: C, 52.65%; H, 2.73%; N, 4.73%. IR (KBr pellet, cm^{-1}): 3362, 3026, 2926, 1684, 1616, 1574, 1523, 1410, 1253, 1170, 972, 935, 842, 746.

Scheme 2. Representation of the Ligands L1 and L2

1,4-(bis(2-pyridylaminomethyl)benzene
L1

1,4-(bis(3-pyridylaminomethyl)benzene
L2
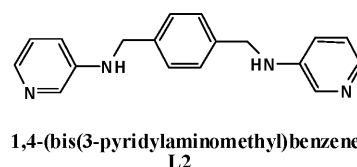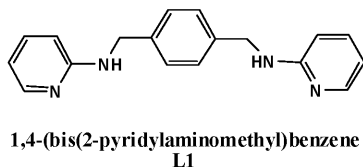
Synthesis of {Co(hfipbb)(L2)$_{0.5}$}$_n$ (2). Compound **2** was prepared by the same procedure as that for compound **1** except that ligand **L2** was used in place of **L1** and the pH of the reaction mixture was adjusted to 7.85. The resulting purple block crystals were collected by filtration in 80.2% yield (based on Co). Anal. Calcd for C$_{26}$H$_{17}$CoF$_6$N$_2$O$_4$ (M_r = 594.35): C, 52.54%; H, 2.88%; N, 4.71%. Found: C, 52.76%; H, 2.84%; N, 4.68%. IR (KBr pellet, cm^{-1}): 3352, 3069, 2914, 1612, 1554, 1494, 1421, 1242, 1018, 986, 848, 779, 725.

Synthesis of {Co(oba)(L1)$_{0.5}$}$_n$ (3). The preparation of complex **3** was similar as above by using CoCl$_2$·6H$_2$O (0.25 mmol, 59.5 mg), H$_2$oba (0.2 mmol, 66.4 mg), ligand **L1** (0.25 mmol, 72.5 mg) in H$_2$O (10.0 mL). The solution pH was adjusted to 8.40 by adding 5 M NaOH. Red block crystals of **3** were obtained in 65.4% yield (based on Co). Anal. Calcd for C$_{23}$H$_{17}$CoN$_2$O$_5$ (M_r = 460.32): C, 60.01%; H, 3.72%; N, 6.08%. Found: C, 60.36%; H, 3.74%; N, 6.12%. IR (KBr pellet, cm^{-1}): 3352, 2920, 2860, 1676, 1599, 1533, 1408, 1257, 1095, 1001, 856, 767, 696, 655.

Synthesis of {Co(oba)(L2)}$_n$·nH$_2$O (4). The preparation of compound **4** is same to that of **3** except that **L2** was used in place of **L1**. The resulting red block crystals were filtered in 64% yield (based on Co). Anal. Calcd for C$_{32}$H$_{28}$CoN$_4$O$_6$ (M_r = 623.51): C, 61.64%; H, 4.52%; N, 8.98%. Found: C, 62.37%; H, 4.14%; N, 9.14%. IR (KBr pellet, cm^{-1}): 3293, 3068, 2843, 1594, 1543, 1413, 1232, 1167, 1019, 879, 783, 646.

Synthesis of {Co(1,2-pda)(L1)$_{0.5}$}$_n$ (5). The compound **5** was prepared following the same procedure as mentioned in compound **3** except that 1,2-H$_2$pda was used instead of H$_2$oba and the pH was adjusted to 7.35. Red block crystals of **5** were obtained in 60.3% yield (based on Co). Anal. Calcd for C$_{19}$H$_{17}$CoN$_2$O$_4$ (M_r = 396.28): C, 57.59%; H, 4.32%; N, 7.06%. Found: C, 57.49%; H, 4.35%; N, 7.24%. IR (KBr pellet, cm^{-1}): 3337, 1611, 1572, 1540, 1403, 1337, 1161, 1079, 1008, 827, 772, 739, 663.

Synthesis of {Co(1,2-pda)(L2)(H$_2$O)}$_n$·nH$_2$O (6). The synthetic procedure was the same as that for **5** except that **L2** was used in place of **L1**. Wine red block crystals of **6** were obtained from the product mixture in 70% yield (based on Co). Anal. Calcd for C$_{28}$H$_{30}$CoN$_4$O$_6$ (M_r = 577.49): C, 58.23%; H, 5.23%; N, 9.70%. Found: C, 58.46%; H, 5.15%; N, 9.66%. IR (KBr pellet, cm^{-1}): 3397, 3315, 2904, 2854, 1600, 1408, 1375, 1298, 1090, 1013, 800, 756, 701, 635, 564, 465.

Single Crystal X-ray Structure Determination of the Compounds 1−6. Single-crystals suitable for structural determination of all the compounds (**1−6**) were mounted on a three circle Bruker SMARTAPEX CCD area detector system under Mo−Kα (λ = 0.71073 Å) graphite monochromated X-ray beam, crystal-to-detector distance 60 mm, and a collimator of 0.5 mm. The scans were recorded with an ω scan width of 0.3°. Data reduction was performed by SAINTPLUS,[17a] empirical absorption corrections using equivalent reflections performed by program SADABS,[17b] structure solution using SHELXS-97[17c] and full-matrix least-squares refinement using SHELXL-97[17d] for the above compounds. All the non-hydrogen atoms were refined anisotropically. Hydrogen atoms on the C atoms were introduced on calculated positions and were included in the refinement riding on their respective parent atoms. Attempts to locate the hydrogen atoms for the solvent water molecules in the crystal structure of compound **4** failed. However, no attempts were made to fix these atoms on their parents. Also attempts to locate the hydrogen atom on nitrogen through Fourier electron density failed in the case of compound **2**. Crystal data and structure refinement parameters for all the compounds (**1−6**) are summarized in Table 1, and selected bond lengths and bond angles are presented in section 3 of Supporting Information. Topological analysis of the compounds are performed by using the TOPOS software.[17e]

■ RESULTS AND DISCUSSION

Synthesis. For a systematic investigation of the effect of ligands **L1** and **L2** on the metal polycarboxylate system, we adopted the hydrothermal technique, as the high temperature and high pressure during the reaction drastically increase the solubility and the reactivity of the reactants. Many factors such

Table 1. Crystal Data and Structural Refinement Parameters for Compounds 1−6

	1	2	3
empirical formula	C$_{26}$H$_{17}$CoF$_6$N$_2$O$_4$	C$_{26}$H$_{17}$CoF$_6$N$_2$O$_4$	C$_{23}$H$_{17}$CoN$_2$O$_5$
formula weight	594.35	594.35	460.32
T (K)/λ (Å)	298(2)/0.71073	298(2)/0.71073	298(2)/0.71073
crystal system	monoclinic	monoclinic	monoclinic
space group	$P2/c$	$P2_1/c$	$P2_1/n$
a (Å)	14.7453(11)	7.5262(7)	13.8015(18)
b (Å)	7.6151(6)	23.884(2)	9.1393(12)
c (Å)	23.8558(17)	14.489(2)	17.045(2)
α (°)	90.00	90.00	90.00
β (°)	102.432(1)	105.395(10)	111.037(2)
γ (°)	90.00	90.00	90.00
volume (Å^3)	2615.9(3)	2511.0(5)	2006.7(5)
Z, ρ_{calcd} (g cm^{-3})	4, 1.509	4, 1.572	4, 1.524
μ (mm^{-1}), $F(000)$	0.734/1200	0.764/1200	0.894/944.0
goodness-of-fit on F^2	0.991	1.031	1.119
R_1/wR_2 [$I > 2\sigma(I)$]	0.0550/0.1216	0.0719/0.1187	0.0566/0.1388
R_1/wR_2 (all data)	0.0658/0.1284	0.1394/0.1451	0.0646/0.1443
largest diff peak/hole (e Å^{-3})	0.458/−0.398	0.442/−0.447	0.694/−0.331

	4	5	6
empirical formula	C$_{32}$H$_{28}$CoN$_4$O$_6$	C$_{19}$H$_{17}$CoN$_2$O$_4$	C$_{28}$H$_{30}$CoN$_4$O$_6$
formula weight	623.51	396.28	577.49
T (K)/λ (Å)	298(2)/0.71073	298(2)/0.71073	298(2)/0.71073
crystal system	monoclinic	monoclinic	triclinic
space group	$P2_1/n$	$P2_1/c$	$P\bar{1}$
a (Å)	12.426(4)	10.783(2)	10.7107(8)
b (Å)	9.771(3)	9.897(2)	11.0699(8)
c (Å)	25.202(8)	15.585(3)	13.0452(10)
α (°)	90.00	90.00	101.866(10)
β (°)	92.962(5)	95.358(2)	104.002(10)
γ (°)	90.00	90.00	110.698(10)
volume (Å^3)	3056.0(16)	1655.9(6)	1329.72(17)
Z, ρ_{calcd} (g cm^{-3})	4, 1.355	4, 1.590	2, 1.442
μ (mm^{-1}), $F(000)$	0.611/1292	1.065/816	0.696/602
goodness-of-fit on F^2	1.100	1.048	1.058
R_1/wR_2 [$I > 2\sigma(I)$]	0.0636/0.1431	0.0298/0.0744	0.0410/0.1011
R_1/wR_2 (all data)	0.0874/0.1550	0.0317/0.0755	0.0460/0.1043
largest diff peak/hole (e Å^{-3})	0.566/−0.272	0.399/−0.202	0.376/−0.185

as pH, temperature, metal−ligand stoichiometry, reaction time, and versatility of metal coordination geometry are all important in the formation of final products. We have taken the d^7 metal ion Co(II) [CoCl$_2$·6H$_2$O] as the metal source in the synthesis of all the compounds. In order to explore the isomeric effect of the secondary ligands **L1** and **L2**, three geometrically different carboxylic acids H$_2$hfipbb, H$_2$oba, and 1,2-H$_2$pda were employed in the reaction system (see Scheme 3). The synthesis of all the compounds were performed at 160 °C in water but as H$_2$hfipbb is highly insoluble in water; assorted solvent water/DMF (5:1) is used in the case of compounds **1** and **2** instead of

4609

dx.doi.org/10.1021/cg300800h | *Cryst. Growth Des.* 2012, 12, 4607−4623

Scheme 3. Synthetic Protocol of the Compounds Presented in the Study
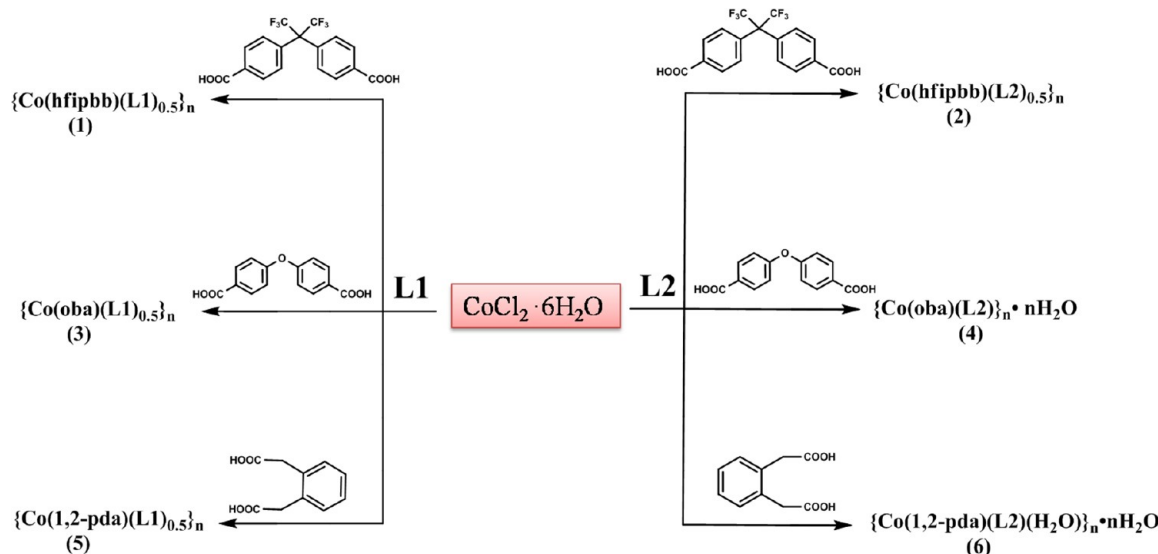

only water. Complexes **1**−**6** are air stable and insoluble in water.

Torsion Angle Measurements to Present the Conformation of L1 and L2. The ligands **L1** and **L2** have two types of flexible groups (i.e., −CH$_2$− and −NH−) as shown in Schemes 1 and 2; as a result, various types of conformations are possible, which create difficulty in assigning the actual conformation of the ligand. Gao et al. explained the conformation of these flexible ligands by measuring the dihedral angle between the pyridine rings.[15c] In our previous report, we have discussed briefly about measuring the torsion angle in the flexible ligand to explain the conformations of the ligand.[8] In this article, in order to explain the actual conformation of the ligands **L1** and **L2**, we have measured two types of torsion angles represented by τ_1 and τ_2. The notation of conformation of the ligand is explained by considering three terms: τ_1–τ_2–m that is explained (see Scheme 5) as follows.

(i) $\tau_1(jkk'j')$ measures the orientation of the −CH$_2$−NH− bond of one side of the xylylene ring with respect to the −CH$_2$−NH− bond of other side of the ring along −(CH$_2$–Ph−CH$_2$)− which offers information of orientation −CH$_2$−NH− bonds whether they exist on the same side or opposite side with respect to the xylylene ring. As shown in the Scheme 5a, the −CH$_2$−NH− bonds can rotate freely to adopt different conformations. If $\tau_1(jkk'j')$ is 180° then both the CH$_2$−NH− bonds are *trans* to each other and if it is 0° they are *cis* to each other. The first term in the notation (τ_1–τ_2–m) is described by this torsion angle. (ii) As shown in the Scheme 5b, apart from the −(CH$_2$−NH)− bond rotation, the NH−Py bond also can rotate freely. $\tau_2(ijj'i')$ gives the skewing of two pyridine rings on −NH− groups through −(NH−CH$_2$−Ph−CH$_2$−NH)− (see Schemes 4 and 5). On the basis of this torsion angle, the orientation of the pyridine rings can be explained by the second term in the notation (τ_1–τ_2–m) of the conformation of the ligand. (iii) Depending on the coordination mode of the nitrogen atom in the pyridine ring to the metal ion, the third term "m" is introduced in the notation (τ_1–τ_2–m). If the both the nitrogen atoms coordinated to the metal ions on the same direction then "m" is termed as *cis* conformation and if it is the opposite direction, then "m" is *trans* conformation. Thus if in a

Scheme 4. Ligand Representing the Location of Vectors at the Flexible Points
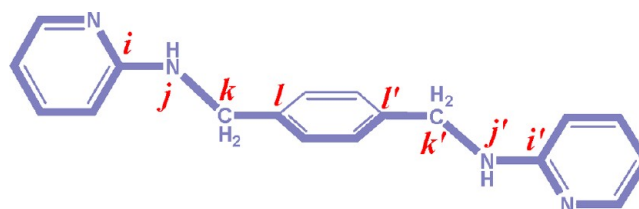

particular case for a ligand **L1** or **L2** the −(CH$_2$−NH)− groups (τ_1) occur on same side with respect to the xylylene ring, the pyridine rings (τ_2) exist on the opposite side and pyridine ring nitrogens (m) coordinate to the metal (cobalt) ions that are located on same side of the ligand, then the conformation of the ligand **L1** or **L2** can be represented by the notation *cis−trans−cis* conformation.

On the basis of the above-mentioned considerations the notation of the conformation of the ligands would be explained in the following sections. Apart from τ_1 and τ_2 values, τ_3 is also measured to explain the deviation of the pyridine rings from the plane of the xylylene ring.

Description of Crystal Structures. *{Co(hfipbb)(L1)$_{0.5}$}$_n$ (1).* Compound **1** crystallizes in the monoclinic space group *P*2$_1$/*c*. As shown in the Figure 1a the molecular diagram consists of a {Co$_2$(COO)$_4$} paddle-wheel in which the apical sites are coordinated to the pyridine nitrogen atoms of two **L1** ligands. Each Co atom in the paddle-wheel is in octahedral geometry constituted by the oxygen atoms from the four hfipbb^{2-} ligands in the basal plane and one nitrogen atom from the **L1** ligand in the apical position, and the other apical positions of the both metal centers are connected to form a long bond between them. The Co−Co bond distance in the dimer is 2.935 Å which is considered to be a long bond. The connectivity of the paddle-wheel along the skeleton of the hfipbb^{2-} units form two-dimensional (2D) interpenetrated helical double layers (Figure 1b).[18] The dihedral angle between the two carboxylate groups on the benzene rings in the bent hfipbb^{2-} is 69.30°, and the separation created between the two paddle-wheels along the hfipbb^{2-} unit is 14.151 Å. The topology of the 2D interpenetrated double layer is a (4,4)

Scheme 5. Representation of Torsion Angles

5a   **5b**
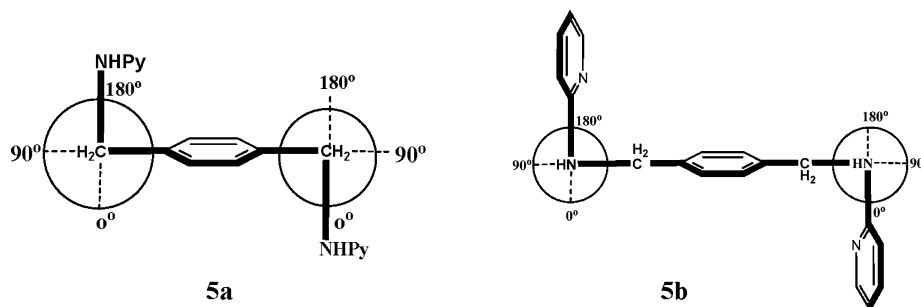
zigzag network with paddle-wheels as the corners and the hfipbb^{2-} as the linkers. The dimensions of the net are 14.15 × 14.15 Å corresponding to the distance between the adjacent centers of dinuclear cobalt paddle-wheels at their corners. The 2D Co−hfipbb sheets are pillared by the ligand **L1** at the apical positions of the Co(II) atoms of the paddle-wheels from the adjacent layers to form a 3D pillared-layered framework. The ligand **L1** connects the paddle-wheels in a *trans−trans−trans* conformation along the crystallographic *a* axis to form 1D chains by creating a separation of 13.09 Å between Co−hfipbb sheets. The −(CH$_2$−NH)− bonds in the ligand **L1** are located in *trans* position with respect to each other with an anti-periplanar torsion angle of 180°, and the two pyridine rings are in *trans* position with respect to each other with an anti-periplanar torsion angle of 180°. Also the nitrogen atoms on the pyridine rings are coordinated to the metal ions in opposite directions. In addition the pyridine rings in the ligand **L1** are deviated with respect to the xylylene ring with a synclinal torsion angle (τ_3) of 67.76° viewed through C20−N2−C21−C22 (Table 3). In our previous article, we reported the compound [Co(hfipbb)(bix)$_{0.5}$]$_n$ in which the Co−hfipbb sheets are linked by the exobidentate ligand 1,4-bis (imidazole-1-ylmethyl)-benzene (bix) which creates the separation of 14.81 Å. From the topological point of view, the present structure can be explained by considering the dicobalt(II) paddle-wheel cluster as a single node which is connected to six such clusters by the linkers hfipbb^{2-} and **L1**. Therefore, the whole network is extended to a 3D six connected 2-fold interpenetrated net with the Schläfli symbol of (4^{12}·6^3) as shown in Figure 1c.

{Co(hfipbb)(L2)$_{0.5}$}$_n$ (2). As shown in Figure 2a, the asymmetric unit in the crystal structure of compound **2** (space group $P2_1/c$) consists of one crystallographically independent Co(II) atom, one hfipbb^{2-} ligand, and half of the **L2** ligand. The coordination geometry around the Co(II) is defined by the four oxygen atoms (O1, O2, O4, and O4#) from four different hfipbb^{2-} units in the equatorial positions, one oxygen atom O3 from hfipbb^{2-}, and nitrogen atom N1 from the **L2** in the axial positions, to form a distorted octahedron. The coordination mode of the two carboxylate groups on the hfipbb^{2-} ligand is different from each other which is responsible for different coordination architecture apart from the regular paddle-wheel SBU architecture. One arm of the carboxylate group in hfipbb^{2-} unit connects to two cobalt atoms in μ_2-η^1:η^1 coordination and the other arm connects to two cobalt atoms with μ_2-η^2:η^0 coordination mode (Figure 2b). This type of coordination modes results in the formation of an eight-membered Co−[O−C−O]$_2$−Co ring along the *ac* plane and four-membered Co−[O]$_2$−Co ring along the *ab* plane; these rings are connected to each other by sharing cobalt atoms to

form 1D zigzag chains through the crystallographic *a* axis as shown in Figure 2c. The connectivity of these chains along the hfipbb^{2-} unit results in the 3D structure in which the 1D chain is running through the *a* axis and the hfipbb^{2-} connected to an eight-membered ring is running through the *c* axis forming Co−hfipbb sheets along the *ac* plane (Figure 2d); the hfipbb^{2-}, connected to a four-membered ring, is running through the *b* axis forming Co−hfipbb sheets along the *ab* plane (Figure 2d). The topology of the Co-hfipbb sheets is same in both the planes, and the connectivity of hfipbb^{2-} is in such a way that one arm is connected to the eight-membered ring and other arm to a four-membered ring in both the *ac* and *ab* planes, respectively. The ligand **L2** again connects the Co atoms of the 1D chains (running along the *a* axis) along the *bc* plane (Figure 2e). Five coordination sites of the metal atom are occupied by the carboxylate oxygens; only one coordination site per metal atom is connected by the ligand **L2** due to which **L2** diagonally connects the Co atoms of the 3D cube with a separation of 15.807 Å in a regular *trans−trans−trans* conformation as explained in the crystal structure of compound **1**. In the ligand **L2**, the pyridine rings are twisted with respect to the xylylene ring with a synclinal torsion angle of 63.14°. The topology of the structure is (4,5) connected network with a Schläfli symbol (4^2.5^2.7^2)(4^2.5^3.7^5).

{Co(oba)(L1)$_{0.5}$}$_n$ (3). The use of H$_2$oba[19] instead of H$_2$hfipbb in the reaction mixture results in the formation of compound **3**. X-ray analysis reveals that compound **3** crystallizes in monoclinic space group $P2_1/n$. As shown in Figure 3a, the molecular diagram consists of dicobalt paddle-wheel SBU in which the coordination geometry of the Co(II) atom is octahedral constituted by the carboxylate oxygen atoms in the basal plane, pyridine nitrogen, and the inter dimer bond in the apical sites. The Co$_2$ SBU in the compound is the same as described in the crystal structure of **1** with Co−O bond lengths in the range of 2.017−2.174 Å, and the intra dimer Co−Co separation is 2.844 Å. The connectivity of the paddle-wheels along the length of the oba^{2-} results in the formation of 2D non-interpenetrated double layers. The dihedral angle between the two carboxylate groups in the oba^{2-} ligand is 80.61°, which is more than the angle between the dihedral angle between the carboxylate groups in the hfipbb^{2-} ligand (69.30°). But the twisting of benzene rings with respect to connecting oxygen atom in the oba^{2-} is more compared to hfipbb^{2-} (see Table 2); as a result the 2D sheets formed in the compound **3** are non-interpenetrated double layers unlike interpenetrated double layers in compound **1**. The skeleton of the double layer is different but the topology of the 2D sheet is the same, which is a (4,4) connected network with dimensions of 13.541 × 13.541 Å (Figure 3b). These 2D sheets are connected by the ligand **L1** in a *trans−trans−trans*
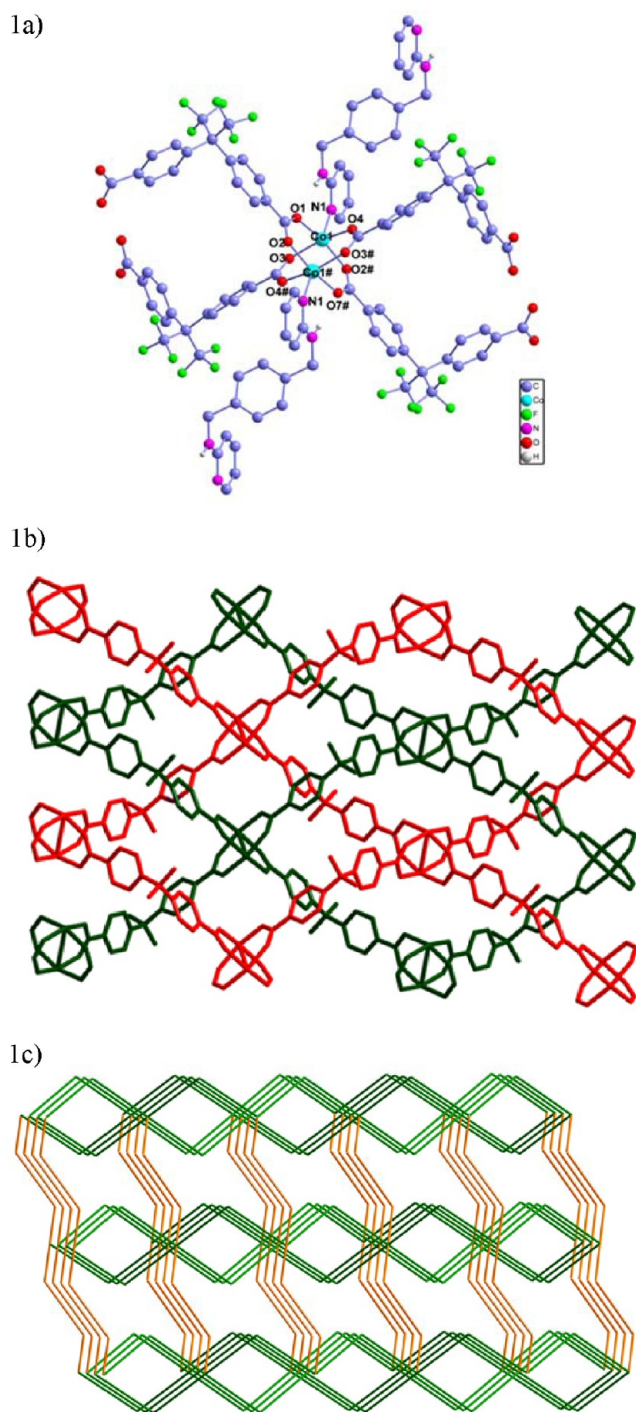
1a)

1b)

1c)

Figure 1. (a) Molecular diagram of compound **1** representing the paddle-wheel. (b) 2D interpenetrated (4, 4)-connected helical double layers. (c) 3D pillared-layered coordination polymer of compound **1** (green color indicates the metal acid layers and yellow color indicates the **L1** ligands as pillars).

conformation to the apical positions of the Co(II) atoms of the paddle-wheels from the adjacent layers to form a 3D extended framework. Interestingly, the pyridine rings in the ligand **L2** are almost in the plane of the xylylene ring with slight deviation of torsion angle 168.46° viewed through C15−N2−C16−C17 (Table 3). The connectivity of the ligand **L2** to the paddle-wheels result in the formation of 1D step chains with a separation of 12.039 Å between the Co(II) atoms of the

paddle-wheels from adjacent layers (Figure 3c). Overall the structure can be viewed as the 1D chains formed by the ligand **L1** which connect the 2D Co−oba sheets to form a 3D pillared layered framework as shown in Figure 3d. By considering the dinuclear paddle-wheel as a single node which is connected to six other clusters through the linkers oba²⁻ and **L1**, the network can be described as a 3D six-connected network with the Schlafli symbol $(4^{12} \cdot 6^3)$ as shown in Figure 3d. From the topological point of view, compounds **1** and **3** have the same topology but the structural parameters are varied by changing the acid from H₂hfipbb to H₂oba.

{Co(oba)(L2)}ₙ·nH₂O (4). Compound **4** crystallizes in monoclinic space group $P2_1/n$. The crystallographically independent Co center is coordinated by four basal donors (four carboxylate oxygen atoms) from two oba²⁻ ligands and two pyridine nitrogen atoms from the ligand **L2** in the apical sites to furnish its octahedral geometry as shown in Figure 4a. The basal Co−O bond lengths consist of two short bonds 2.035, 2.042 Å and two long bonds 2.348 and 2.297 Å. The apical Co−N bond lengths are 2.085 and 2.090 Å. In this compound, the ligand **L2** exists in *cis−cis−trans* conformation in which the −(CH₂−NH)− bonds and pyridine rings are located on the same side of the benzene ring and the nitrogen atoms are pointed toward different directions (Figure 4b). The −(CH₂−NH)− bonds in the ligand **L2** are to found to be in *cis* position with respect to each other with a synclinal torsion angle of 50.81°, and the pyridine rings are also found to be in *cis* position with respect to each other with a synclinal torsion angle of 51.93°, but the nitrogen atoms in the pyridine rings are coordinated to metal ions in the *trans* direction. The pyridine rings in the ligand **L2** are deviated with respect to the xylylene ring to different extents with a synclinal torsion angle of 63.07 and antiperiplanar torsion angle of 163.57. The *cis−cis−trans* conformation adopted by ligand **L2** results in the formation of [Co₂L2₂] loops as shown in Figure 4c. The separation created by ligand **L2** between the metal centers in the loop is 9.076 Å. Each loop acts as a four connector and connects the four other loops via oba²⁻ units (Figure 4d). The Co atoms in the loops are in tetrahedral geometry (ignoring long Co−O bonds) in which two sites are occupied by nitrogen atoms and the remaining two sites in the tetrahedral geometry are occupied by the oba²⁻ to furnish a 2D network. Each Co atom is connected to three other Co atoms in which two are connected by oba²⁻ and other is connected by a pair of **L2** ligands. The coordination mode of the carboxylate groups on the oba²⁻ ligand is μ_1-η^1:η^1, the dihedral angle between the two benzene rings is 87.22°, and the separation created by the oba²⁻ between the two metal centers along the skeleton of the ligand is 14.170 Å. The connectivity of the oba²⁻ ligands to metal centers results in the formation of 1D chains, running through the crystallographic *c* axis connecting the [Co₂L2₂] loops. These 1D chains thread the loops to form a 2D extended network as shown in Figure 4e. From a topological point of view, the network topology features a 3-connected net with (6,3) topology. Batten et al. and Zheng et al. reported the networks with the same topology (6,3) in which the loops are connected by the rods to form a 2D network and a pair of identical 2D single nets is interlocked with each other in a 2D → 2D parallel fashion, thus directly leading to the formation of a 2D polyrotaxane-like structure containing rotaxane-like motifs.[20] Employing a long rigid ligands such as bpea and bpdc in the compounds, reported by a Batten and Zheng, results in 2D polyrotaxane-like structures, whereas in the present study, the
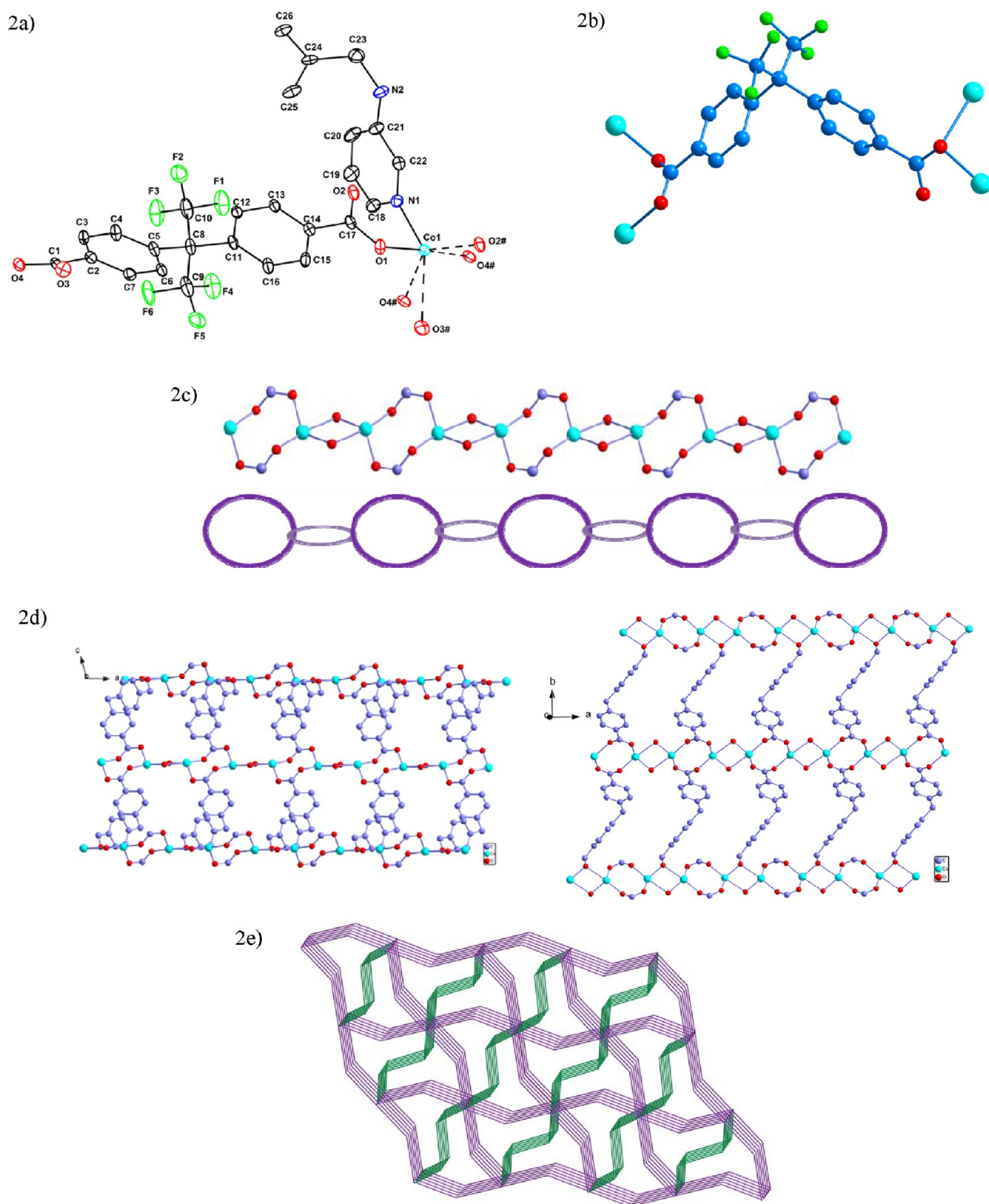
2a)

2b)

2c)

2d)

2e)

Figure 2. (a) ORTEP view of the basic unit of **2**. Hydrogen atoms are removed for clarity. Thermal ellipsoids are at the 30% probability level. (b) Two different coordination modes of the carboxylate groups (μ_2-η_1:η_1 and μ_2-η_2:η_0) in the hfipbb^{2-} ligand. (c) 1D zigzag chain formed due to Co–[O–C–O]$_2$–Co and Co–[O]$_2$–Co rings and its representation. (d) 2D layers formed by the connectivity of hfipbb to the 1D zigzag chains along the ac and ab planes. (e) 3D topological representation of compound **2** (violet color indicates the 3D metal acid coordination architecture and green color indicates the diagonal connectivity of ligand **L2**).
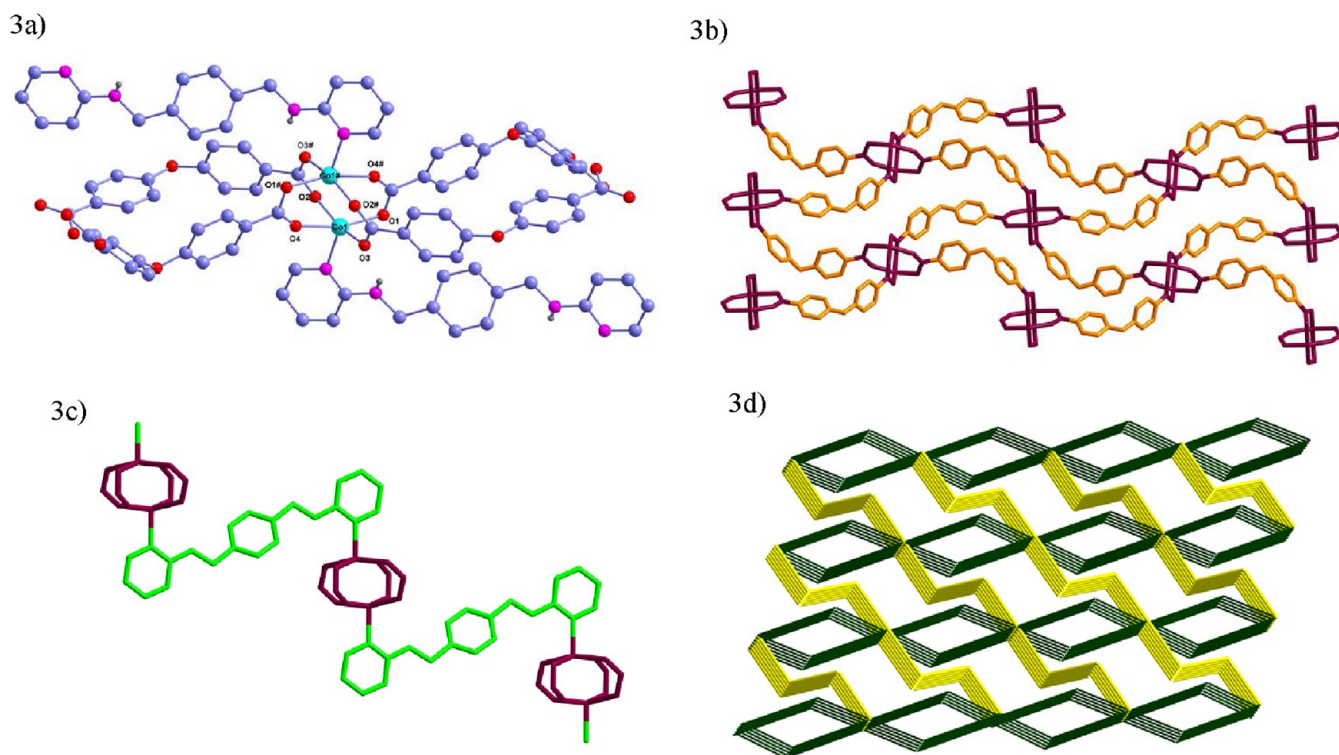
4613

dx.doi.org/10.1021/cg300800h | *Cryst. Growth Des.* 2012, 12, 4607−4623

3a)

3b)

3c)

3d)

Figure 3. (a) Molecular diagram of compound **3** showing the hexapodal paddle-wheel. (b) 2D (4,4)-connected non-interpenetrated double layers formed due to connectivity of oba^{2-} and metal centers. (c) 1D chains formed by the connectivity of paddle-wheels with ligand **L1**. (d) Topological representation of 3D layered-pillared structure of compound **3** (green color indicates the metal acid layers and yellow color indicates the pillars **L1** ligands).

Table 2. Dihedral and Twisting Angles in the Carboxylic Acids

acid	hfipbb^{2-}		oba^{2-}		pda^{2-}	
compound	**1**	**2**	**3**	**4**	**5**	**6**
dihedral angle λ (Å)	70.55	63.33	80.61	71.07	25.12	19.81
twisting angle θ (Å)	132.56/81.46	103.33/112.45	130.17/19.40	99.36/90.86		

Table 3. Torsion Angles and the Corresponding Conformations of the Ligands L1 and L2 in Compounds 1–6

C. no.	ligand	τ_1 (Å)	τ_2 (Å)	τ_3/τ'_3 (Å)	conformation
1	L1	180	180	67.76/−67.76	trans−trans−trans
2	L2	180	180	63.14/−63.14	trans−trans−trans
3	L1	180	180	168.50/−168.50	trans−trans−trans
4	L2	50.81	51.93	163.23/−63.15	cis−cis−trans
5	L1	180	180	74.53/−74.53	trans−trans−trans
6	L2	51.97	168.50	96.13/−74.85	cis−trans−cis

semirigid bent ligand oba^{2-} does not allow the nets to interlock each other resulting in the formation of a 2D structure in which the 1D chains connect loops.

{Co(1,2-pda)(L1)$_{0.5}$}$_n$ (**5**). Use of 1,2-H$_2$Pda instead of bent carboxylic acids (H$_2$hfipbb and H$_2$Oba in compounds **1** and **3**, respectively) result in the formation of 3D coordination polymer **5**. X-ray analysis reveals that compound **5** crystallizes in a monoclinic system with space group $P2_1/c$. As shown in Figure 5a, the molecular diagram consists of a six-connected dicobalt paddle-wheel [Co$_2$(pda)$_4$(L1)$_2$] in which the coordi-

nation geometry of the Co(II) atom is octahedral constituted by the four carboxylic oxygen atoms from four different pda^{2-} ligands in the basal plane, one nitrogen atom from the ligand **L2** in the apical position, and the other apical positions of the two Co(II) atoms are shared by a bond between them. In the Co$_2$ SBU the bond distances between the Co and the carboxylic oxygen atoms lie in the range of 2.017−2.162 Å and the intra dimer Co−Co bond distance is 2.858 Å. pda^{2-} exists in the *trans* conformation with acetate groups twisted with respect to each other with a torsion angle of 156.72 Å (viewed through C3−C9−C19−C18).[21] The connectivity of the pda^{2-} units to the paddle-wheel result in the formation of 2D Co−pda sheets with (4,4) connected network topology as shown in Figure 5b. The distance between the paddle-wheels along the length of the pda^{2-} is 9.23 Å (viewed through the center of the adjacent metal atoms in the paddle-wheel). Unlike H$_2$hfipbb and H$_2$Oba ligands, H$_2$pda is not a bent ligand, and the dihedral angle between the two carboxylate groups is 27.32°. These features allow the pda^{2-} to form (4,4) connected single planar sheets rather than double layers as in the case of compounds **1** and **3**. These 2D Co−pda sheets are pillared by the ligand **L1** to form 3D pillared layered structure as described in the compounds **1** and **3** (Figure 5c). The ligand **L1** connects to the apical positions of the Co(II) of the paddle-wheels from the adjacent layers in a regular *trans−trans−trans* conformation by

4a)

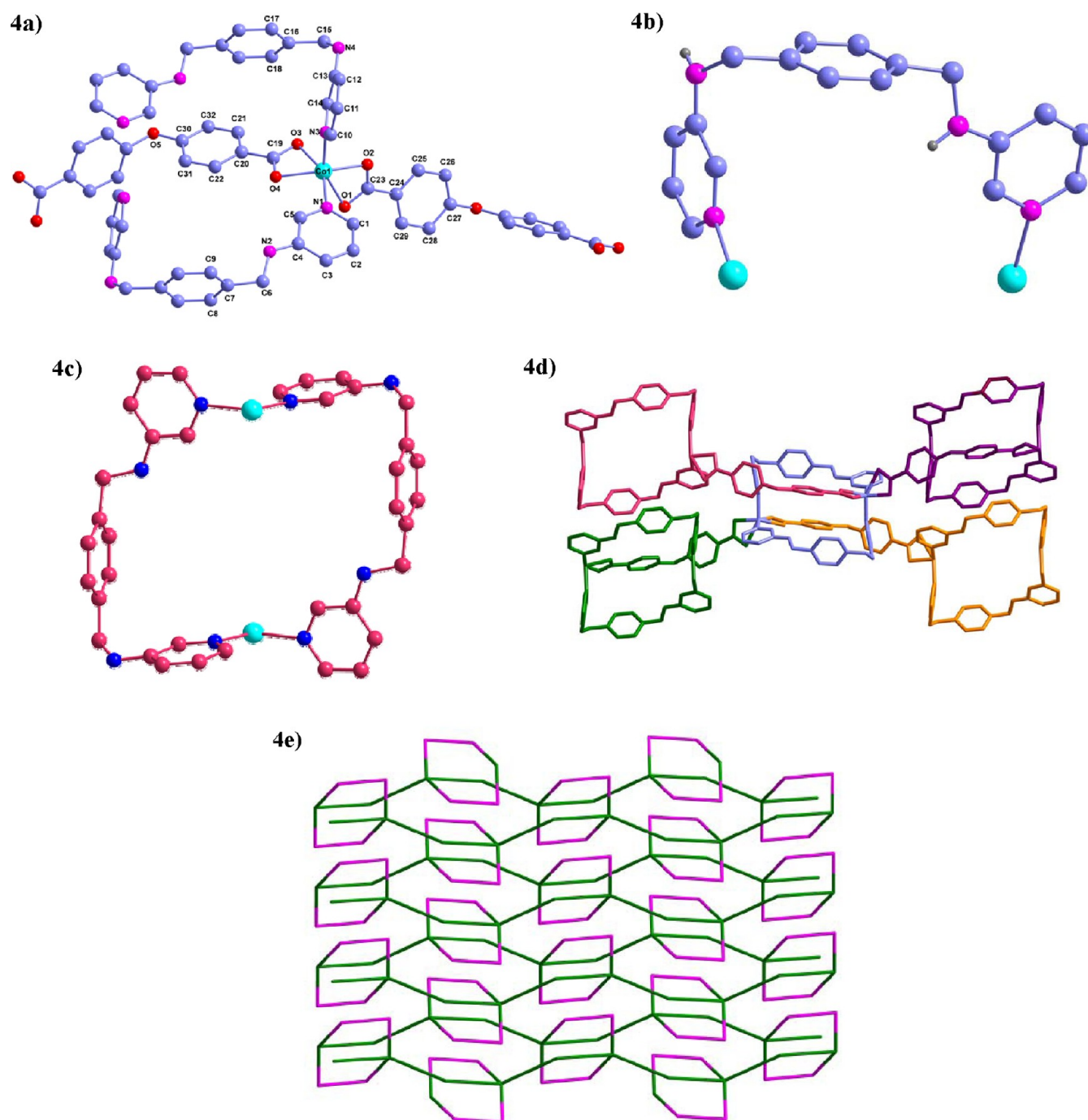

4b)

4c)

4d)

4e)

Figure 4. (a) Coordination environment around the Co(II) ion in compound **4**. (b) *cis−cis−trans* conformation of the ligand **L2**. (c) $[Co_2L2_2]$ loops formed due to the *cis−cis−trans* conformation of the ligand **L2**. (d) Tetrapodal connectivity of $[Co_2L2_2]$ loops. (e) Topological representation of the 2D layer formed by the connectivity of loops and oba²⁻.

creating a separation of 12.989 Å between the two layers. The pyridine rings in the ligand **L1** are deviated from the xylylene ring with a torsion angle of 74.53° (Table 3). From the topological point of view, dicobalt paddle-wheel is considered as single node, and the pda²⁻, ligand **L1** are considered as linkers. Each node is connected to six nodes and the each linker bridges two nodes thereby forming a six connected net with a Schlafli symbol of $(4^{12} \cdot 6^3)$ as shown in Figure 5c. The topology of the networks formed in compounds **1**, **3**, and **5** is the same.

{Co(1,2-pda)(L2)(H₂O)}ₙ·nH₂O (**6**). Compound **6** crystallizes in the triclinic space group $P\bar{1}$. As illustrated in Figure 6a, each

Co(II) atom is six coordinated by three oxygen atoms from the two pda²⁻ ligands and the two nitrogen atoms from two different **L2** ligands and one oxygen atom from the aqua ligand forming a distorted $[CoN_2O_3(H_2O)]$ octahedral geometry. Each pda²⁻ anion coordinates to two Co(II) atoms with μ_1-η^1:η^1 and μ_1-η^1:η^0 bridging modes on either side in a typical *cis* conformation to form a molecular box $[Co_2(pda)_2]$ as shown in Figure 6b. Both acetate side chains in the pda²⁻ twist with respect to each other with synperiplanar torsion angle of 22.22° viewed through C1−C2−C9−C10. Each molecular box connects to other boxes through two pairs of ligand **L2**. The
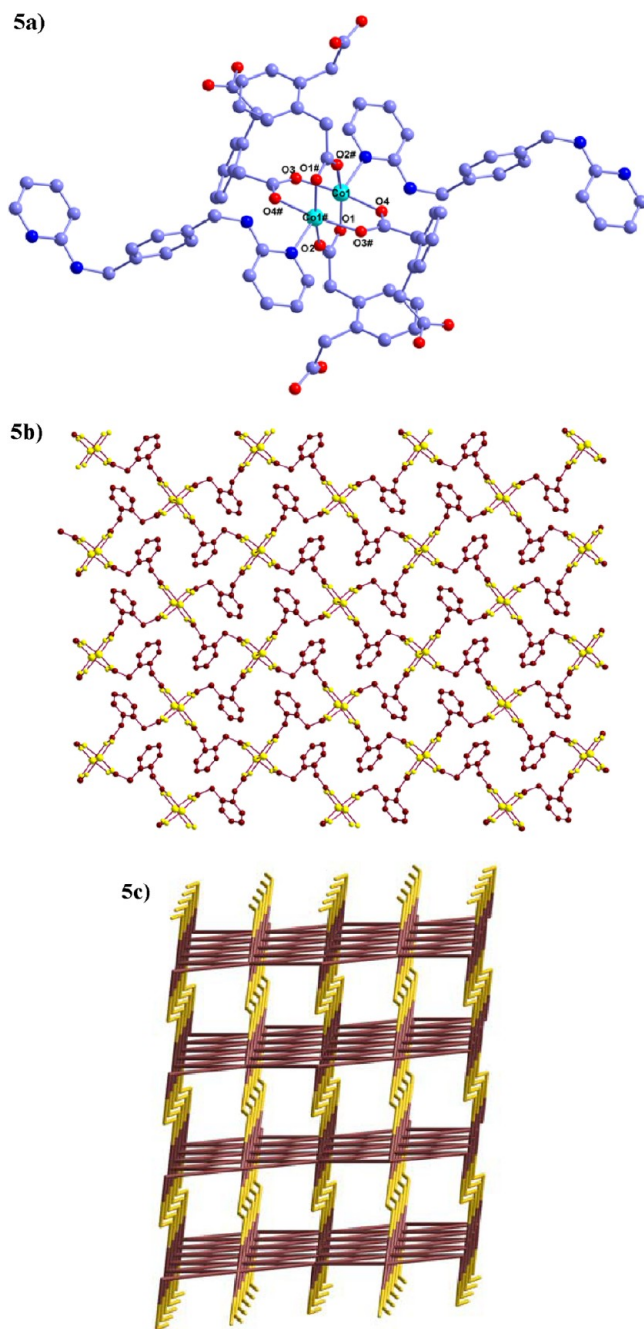
5a)

5b)

5c)

Figure 5. (a) Paddle-wheel molecular diagram of compound **5**. (b) 2D (4,4)-connected single layer formed by the connectivity of pda^{2-} and the Co(II) metal centers. (c) Topological representation of 3D coordination polymer of compound **5** viewing the pillared-layered architecture (brown color indicates the 2D single layer and yellow color indicates the **L1** ligands as pillars).

ligand **L2** connects the metal centers of the adjacent molecular boxes in unusual *cis−trans−cis* fashion to form 1D chains. Here the −CH$_2$−NH− groups are arranged *cis* to each other with synclinal torsion angle of 51.97°, but interestingly the pyridine rings at −NH− groups are located *trans* to each other with an anti-periplanar torsion angle of 168.52° and the nitrogen atoms in the pyridine rings are coordinated to metal atoms in a typical *cis* direction. Additionally, the pyridine rings in the ligand **L2** are deviated with respect to the xylylene ring by angles of 74.94° and 96.11°. The separation created by the ligand **L2**

between the metal centers is 12.387 Å. These chains connect the molecular boxes to form a 1D ladder-like structure as shown in Figure 6c. The *trans* conformation of pda^{2-} in compound **5** is changed to *cis* conformation in compound **6** by changing the secondary ligand from **L1** to **L2**. The conformational modulation of *trans* to *cis* form is achieved by the rigid secondary ligands as described in some literature.[22] But the compounds **5** and **6** are the examples in which the conformational modulation is achieved by the change in the position of the ligating atom in the flexible secondary ligand. Because of the presence of one lattice water, a classical hydrogen bonding is observed between the N−H groups of ligand **L2** from one ladder and lattice water molecule and then to the carboxylate oxygen atom of another ladder to form a 2D supramolecular network as shown in Figure 6d.

Factors Affecting the Structural Diversities in the Compounds 1−6. *Effect of Geometry of Carboxylic Acid.* We have used three geometrically different bent dicarboxylic acids H$_2$hfipbb, H$_2$oba, and H$_2$pda with the secondary linker **L1** which results in the formation of compounds **1**, **3**, and **5** with general formula [M(acid)(**L1**)$_{0.5}$]$_n$. In these compounds, dinuclear paddle-wheels [Co$_2$(O$_2$CR)$_4$] are formed and the connectivity of the paddle-wheels along the length of the acids results in the formation of 2D sheets with a (4,4)-connected rhombic window. In compound **1**, a unique helical interpenetrated double layer is formed in which left and right helical chains appear. In compound **3**, even though the carboxylic acid is bent, a 2D non-interpenetrated double layer is formed, whereas in **5** a single layer is only formed because the carboxylate groups are almost planar. The structural variation among the 2D sheets formed in these compounds is mainly due to twisting of the benzene rings with respect to the central bridging atom in the bent carboxylic acids. The hfipbb^{2-} ligand in **1** exists in V-shaped conformation with a dihedral angle of 70.55° between two carboxylate groups, and the two benzene rings are twisted with respect to each other through the bridging carbon atom by torsion angles of 132.56° (viewed through C15−C12−C8−C5) and 81.46° (viewed through C1−C2−C8−C9). The oba^{2-} ligand in **3** exists in stretched V-shaped conformation with a dihedral angle of 80.61°, and the benzene rings are twisted with respect to each other through bridging oxygen atoms by a torsion angles of 130.17° (viewed through C1−C2−O5−C8) and 19.40° (viewed through C20−C21−O5−C5). The twisting of the benzene rings in hifpbb^{2-} is lesser in comparison to that in oba^{2-}, which is mainly due to the presence of bulky CF$_3$ groups on the bridging carbon atom, thereby restricting the free twisting of the benzene rings and resulting in the formation of 2D interpenetrated layers, while oba^{2-} forms a non-interpenetrated double layer. The dihedral angle between the two carboxylate groups in the pda^{2-} is 25.12° indicating the coplanarity of the carboxylate groups and forms 2D single layers unlike double layers. When **L2** is used as secondary ligand with carboxylic acids H$_2$hfipbb and H$_2$oba in compounds **2** and **4** respectively, the benzene rings are twisted with respect to each other to lesser extent, that is, 103.33° and 112.45° in hfipbb^{2-} and 99.36° and 90.86° in oba^{2-}. The variation in the 2D layers, formed, is shown in the Figure 7. Dihedral angles and the twisting angles of the acids employed in the compounds are presented in Table 2.

Effect of Position of the N Atom in the Pyridyl Ring. Dinuclear paddle-wheels are formed in compounds **1**, **3**, and **5** when **L1** is the secondary ligand, but with the same carboxylic acids different coordination architectures are formed apart from

6a)

6b)
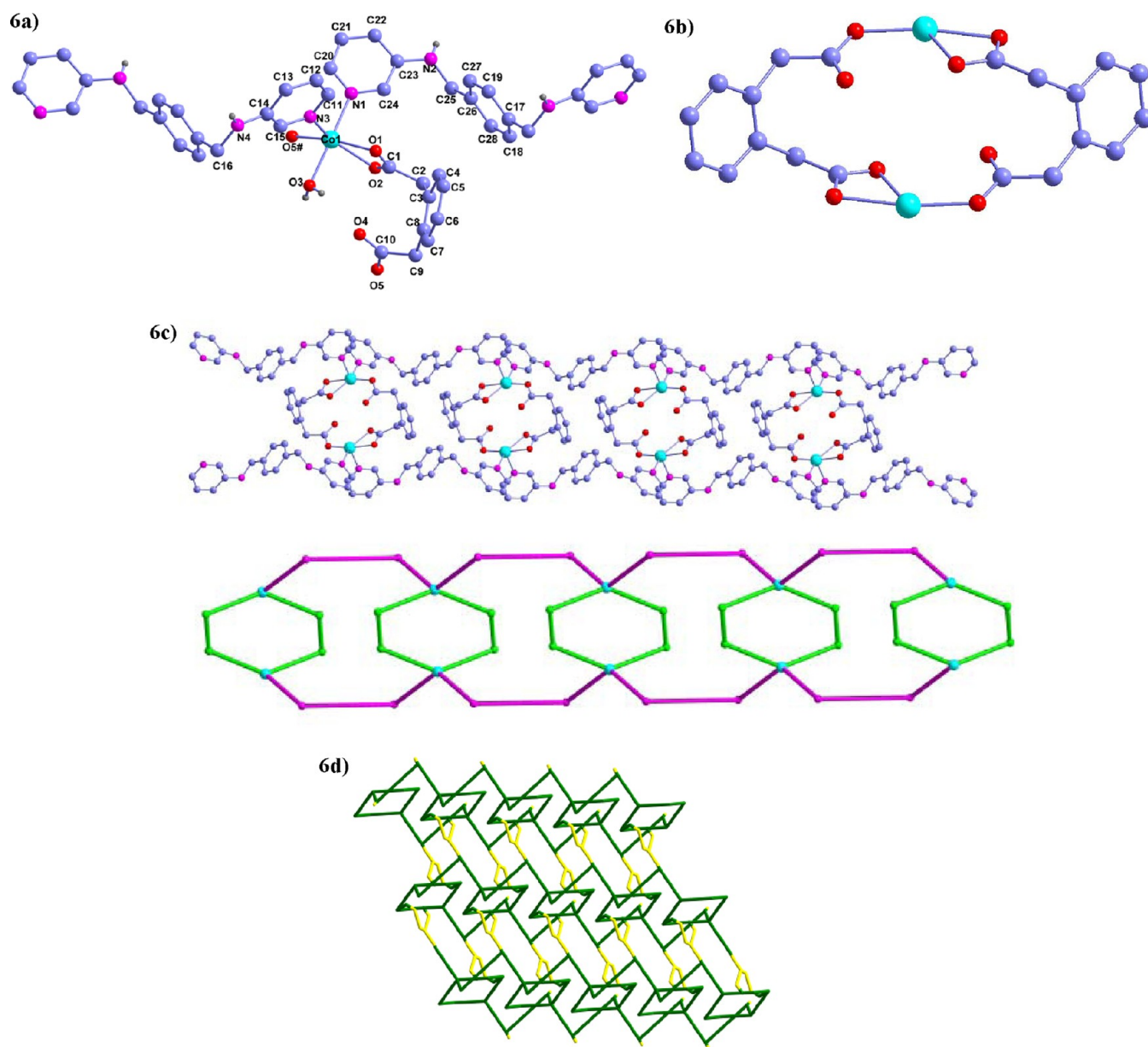

6c)

6d)

Figure 6. (a) Coordination environment of the Co(II) ion in compound **6**. (b) Molecular box $[Co_2(pda)_2]$ formed by the cis conformation of pda^{2-}. (c) 1D ladder formed by the connectivity of molecular boxes with the ligand **L2**, and its topological representation. (d) Topological representation of 2D supramolecular network formed due to classical hydrogen bonding interactions among the 1D ladders through the lattice water molecule (yellow color indicates the hydrogen bonding between the two ladders through solvent water molecule).

the paddle-wheels when **L2** is used as a secondary ligand in compounds **2**, **4**, and **6**. This structural variation can be explained in the light of steric hindrance created at the metal coordination sphere. In all compounds, the four coordination sites of the metal octahedron are occupied by the oxygen atoms of the carboxylic acids. In the compounds where the fifth coordination site is connected to the nitrogen atom of the secondary ligand **L1**, in which the long bulky PXA group, that is, −NH−CH$_2$−C$_6$H$_5$−CH$_2$−NH−, is attached to the pyridine ring in the second position with respect to the coordinated nitrogen atom, the steric hindrance or crowdedness at the metal coordination sphere increases which does not permit another **L1** ligand to enter into the residual coordination site. Thus, the presence of ligand **L1** in compounds **1**, **3**, and **5** allocates only a long metal to metal bond in the sixth position which favors the formation of paddle-wheels. However, in ligand **L2** the bulky

PXA group is at the third position with respect to the coordinated nitrogen atom which diminishes the magnitude of steric hindrance or crowdedness at the metal coordination sphere compared to **L1** which permits the other ligand to connect with the metal atom. Hence in compound **2**, the metal coordination sphere containing ligand **L2** allows the fifth carboxylate oxygen atom (by now four carboxylate oxygen atoms are presented in the coordination sphere) to connect to the Co(II) atom with a Co−O bond length of 2.693 Å, and moreover in compounds **4** and **5** it has become possible for another ligand **L2** to enter into the metal coordination sphere through the Co−N bond. In the previous literature, Gao et al. reported the Cd complexes where also we can observe that the seven-coordinated Cd(II) ion contains three pyridyl N atoms from three different **L1** ligands in the $[Cd(L1)_{1.5}(NO_3)_2]_n$ complex, whereas the six-coordinated Cd(II) ion has four
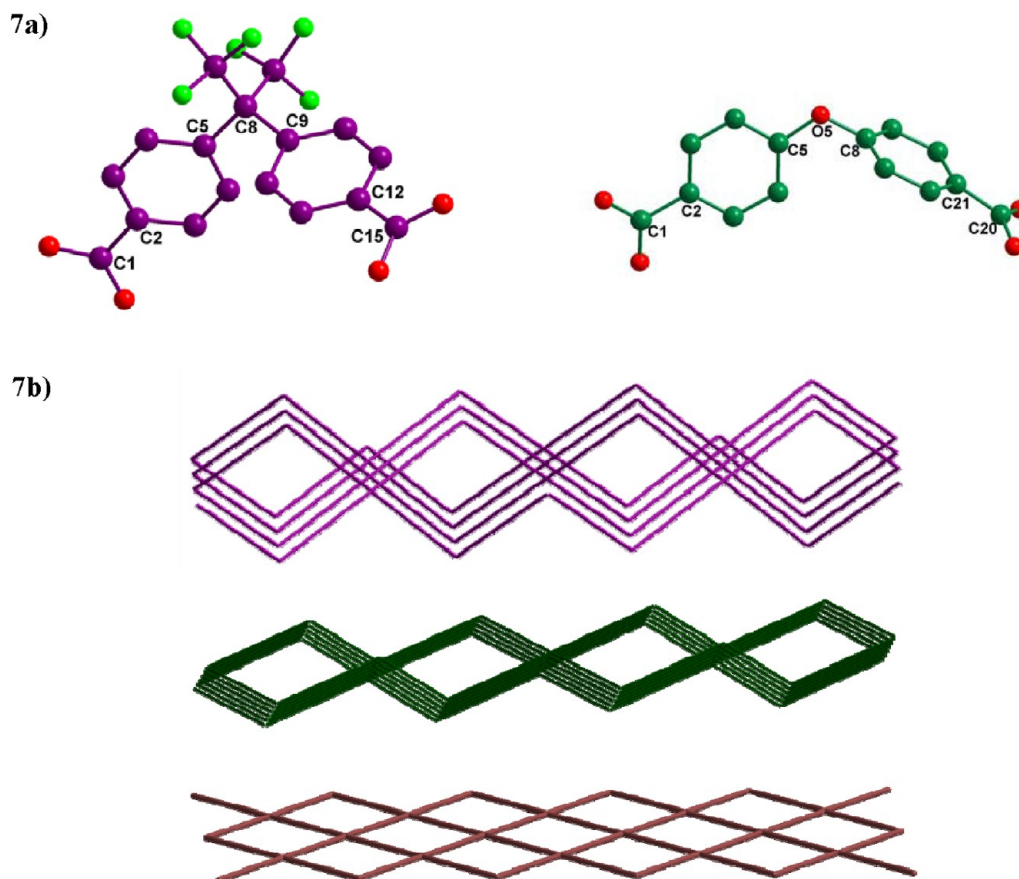
Figure 7. (a) Atom labeling diagram of the ligands hfipbb^{2-} (left) and oba^{2-} (right) in measuring the twisting angles. (b) Variation in the 2D layers formed in the compounds: 2D interpenetrated helical double layers **1** (top) 2D non-interpenetrated double layers **3** (middle) and 2D single layer in **5** (bottom).

pyridyl N atoms from four different **L2** ligands in the $[Cd(\mathbf{L2})_2(NO_3)_2]_n$ complex.[15c] These compounds also support that ligand **L1** generates more crowdedness than ligand **L2**, and consequently the accommodation of the other ligands into the metal coordination sphere is also affected as shown in Figure 8.
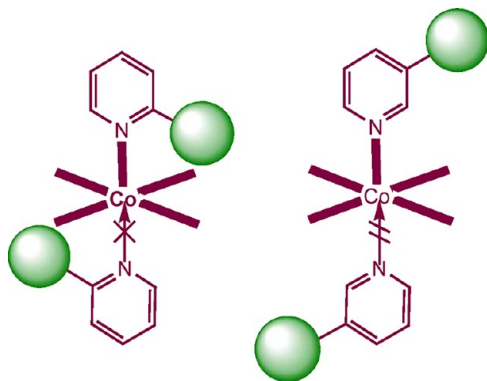

Figure 8. Figure showing the effect of bulkiness of the secondary ligand at the metal coordination sphere.

Effect of Conformation of the Secondary Ligand. The conformation of the secondary ligand has an essential role in the formation of final products. Ligand **L1** exists only in *trans–trans–trans* conformations in compounds **1**, **3**, and **5** and favors the formation of paddle-wheels. The coordination sphere around the metal ions in these compounds allows ligand **L1** to

be in the *trans–trans–trans* conformation only. But ligand **L2** exists in three completely different conformations in compounds **2**, **4**, and **6** respectively. The major factor, accountable for the modulation of different conformations of **L2**, is attributed to the accommodation of two secondary ligands in the coordination sphere of the metal ions in these compounds. To meet the coordination requirements at the coordination sphere of the metal polyhedral imposed by the carboxylate groups, ligand **L2** exists in three different conformations, that is, *trans–trans–trans* in **2**, *cis–cis–trans* in **4**, and *cis–trans–cis* in **6**. In compound **4**, $[Co_2L2_2]$ loops are formed due to the *cis–cis–trans* conformation of the ligand **L2**, and in compound **6**, the $[Co_2(pda)_2]$ molecular boxes are connected by ligand **L2** in a remarkable *cis–trans–cis* conformation. In Co-pda system, the flexible secondary ligand **L1** in *trans–trans–trans* conformation allows the pda^{2-} in regular *trans* conformation in compound **5**, whereas **L2** in *cis–trans–cis* conformation allows the pda^{2-} to adopt the rare *cis* conformation which is usually obtained by the rigid secondary ligands. The torsion angles of the ligands at the flexible groups on the scale are shown in Figure 9 and tabulated in Table 3.

XRPD and Thermogravimetric Analysis (TGA). To ensure the phase purity of the products, X-ray powder diffraction data for all the compounds have been recorded. Similar diffraction patterns for the simulated data (calculated from single crystal data) and observed data prove the bulk homogeneity of the crystalline solids (see Supporting Information for the PXRD patterns of compounds **1**–**6**). Although the experimental patterns have a few unindexed diffraction peaks and some are
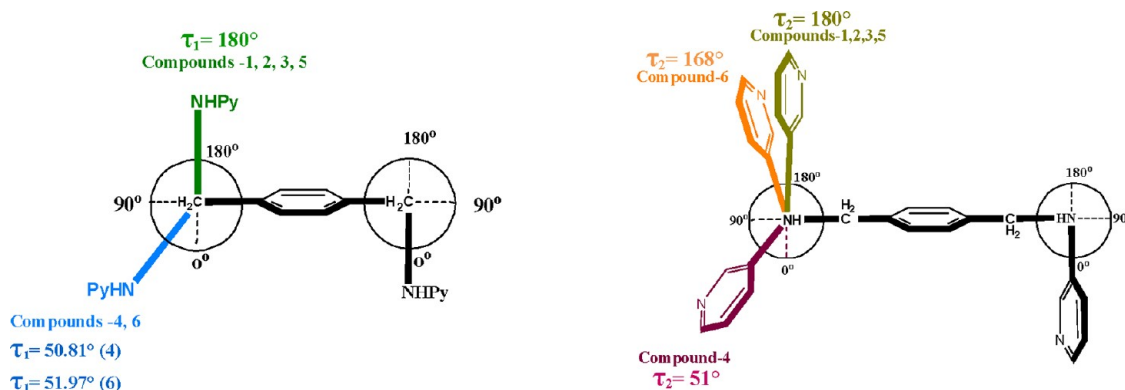
Figure 9. Representation of orientation of the flexible groups −(CH2−NH)− (right) −(NH−Py)− (left) in the ligands **L1** and **L2** in the compounds **1**−**6** based on torsion angle.

slightly broadened and shifted in comparison to those simulated from the single-crystal data, it can still be regarded that the bulk as-synthesized materials represent compounds.

TGA curves are made under flowing N_2 for crystalline samples **1**−**6** in the temperature range 30−800 °C (Section 1c, Supporting Information). Compound **1** exhibits thermal stability up to 250 °C and undergoes continued weight loss which is attributed to decomposition of organic ligands hfipbb[2−] and **L1**. Compounds **2** and **3** show thermal stability up to 395 and 370 °C respectively and undergoes continual weight loss due to pyrolysis of organic ligands. Compound **4** shows thermal stability up to 310 °C with loss of one lattice water molecule and undergoes decomposition corresponding to the organic ligands oba[2−] and **L2**. Compound **5** is stable up to 350 °C and loses the organic ligands continuously upon heating. Compound **6** loses the solvent water molecule and coordinated water molecule up to the temperature 135 °C with weight loss of 5.95% (calcd. 6.22%) and the framework is stable up to 240 °C and undergoes continuous weight loss.

Electronic Properties. Solid state diffuse reflectance (electronic absorption) spectra for the compounds **1**−**6** are presented in Section 1d, Supporting Information. The absorption peaks at 593, 468, 324, 225 nm (compound **1**), 590, 340, 225 nm (compound **2**), 580, 476, 320, 223 nm (compound **3**), 542, 337, 224 nm (compound **4**), 580, 470, 320, 226 nm (compound **5**), and 580, 336, 225 nm (compound **6**) are observed in the respective spectra. In the case of compounds **1**, **3**, and **5** along with the expected transitions, another type of transition has been observed in the region 460−475 nm which is absent in the case of compounds **2**, **4**, and **6**. Compounds **1**, **3**, and **5** have paddle-wheel structure in common, where the paddle-wheel is formed by cobalt−cobalt weak interactions (long Co−Co bond). We believe that the absorption maxima in the region of 460−475 nm for **1**, **3**, and **5** originate from an energy gap that is caused by weak cobalt−cobalt interactions in respective paddle-wheels. In all the spectra, the lowest energy bands are assigned due to d−d transitions of Co(II) metal ions and the highest energy bands are due to π−π* transitions from phenyl groups which are comparable with the electronic spectra of free ligands.

Magnetic Properties. In all the compounds, Co^{2+} ions linked by the carboxylate bridges lead to the magnetic interactions among metal centers. The magnetic susceptibility measurements of the polycrystalline compounds were performed under an applied field of 2000 Oe over the temperature range 2−300

K. The magnetic behavior of compounds **1**−**5** are presented in the form of χ_M vs T and $\chi_M T$ vs T in Figure 10.

Compound 1. The temperature-dependent on magnetic susceptibility is presented as χ_M vs T and $\chi_M T$ vs T plots in Figure 10a. The magnetic susceptibility (χ_M value) of compound **1** increases with decreasing temperature and a broad maximum has been observed at around 100 K and then after 16 K sharply increases up to 2 K. The nature of the χ_M vs T curve observed for compound **1** is similar to that observed for compound Co(endi)(N3)$_2$ in the literature.[23] At room temperature (300 K), $\chi_M T$ value is 4.74 cm^3 K mol^{-1}, which is higher than the spin-only value for two isolated Co(II) atoms (3.75 cm^3 K mol^{-1}, g = 2.0). Upon cooling, the $\chi_M T$ value decreases continuously to 0.049 cm^3 K mol^{-1} at 2 K. The nature of the $\chi_M T$ vs T plot suggests a dominant antiferromagnetic exchange between the two Co^{II} ions and the strong spin−orbital coupling through the ^4T_g state of the octahedral Co(II) center. The structure of compound **1** reveals that the antiferromagnetic exchange between the two Co^{2+} ions is transmitted through the −O−C−O− bridges in the Co-paddle-wheels. We tried to fit the susceptibility curve with the simple isolated dimer equation, but we could not succeed due to a large hump observed in the susceptibility curve.

Compound 2. Figure 10b shows the temperature dependence of χ_M and $\chi_M T$ values for compound **2**. The room temperature $\chi_M T$ value (2.79 cm^3 K mol^{-1}) is higher than the expected value for isolated Co(II) ions. The $\chi_M T$ value gradually decreases upon cooling and reaches a minimum value 0.096 cm^3 K mol^{-1} at 2 K. The $1/\chi_M$ vs T plot above the 80 K follows the Curie−Weiss law with negative Weiss constant Θ = −43.55 K. The above features indicate antiferromagnetic exchange between the neighboring Co(II) centers. As observed in the crystal structure analysis, the magnetostructure for compound **2** can be considered as a 1D chain formed by the alternate eight-membered and four-membered rings bridged by the double carboxyl and double oxo groups resulting in the two types of exchange pathways. Because of the lack of a suitable model for such a system with alternating bridges, the relevant exchange parameters could not be estimated. But the nature of the exchange phenomenon observed in this compound is consistent with the previously reported 1D Co(II) chains containing compounds with two exchange pathways.[24]

Compound 3. Both χ_M vs T and $\chi_M T$ vs T plots of compound **4** are presented in Figure 10c. The room temperature $\chi_M T$ value of compound **3** is 5.65 cm^3 K mol^{-1}, which is much higher than the spin only value of 3.75 cm^3 K
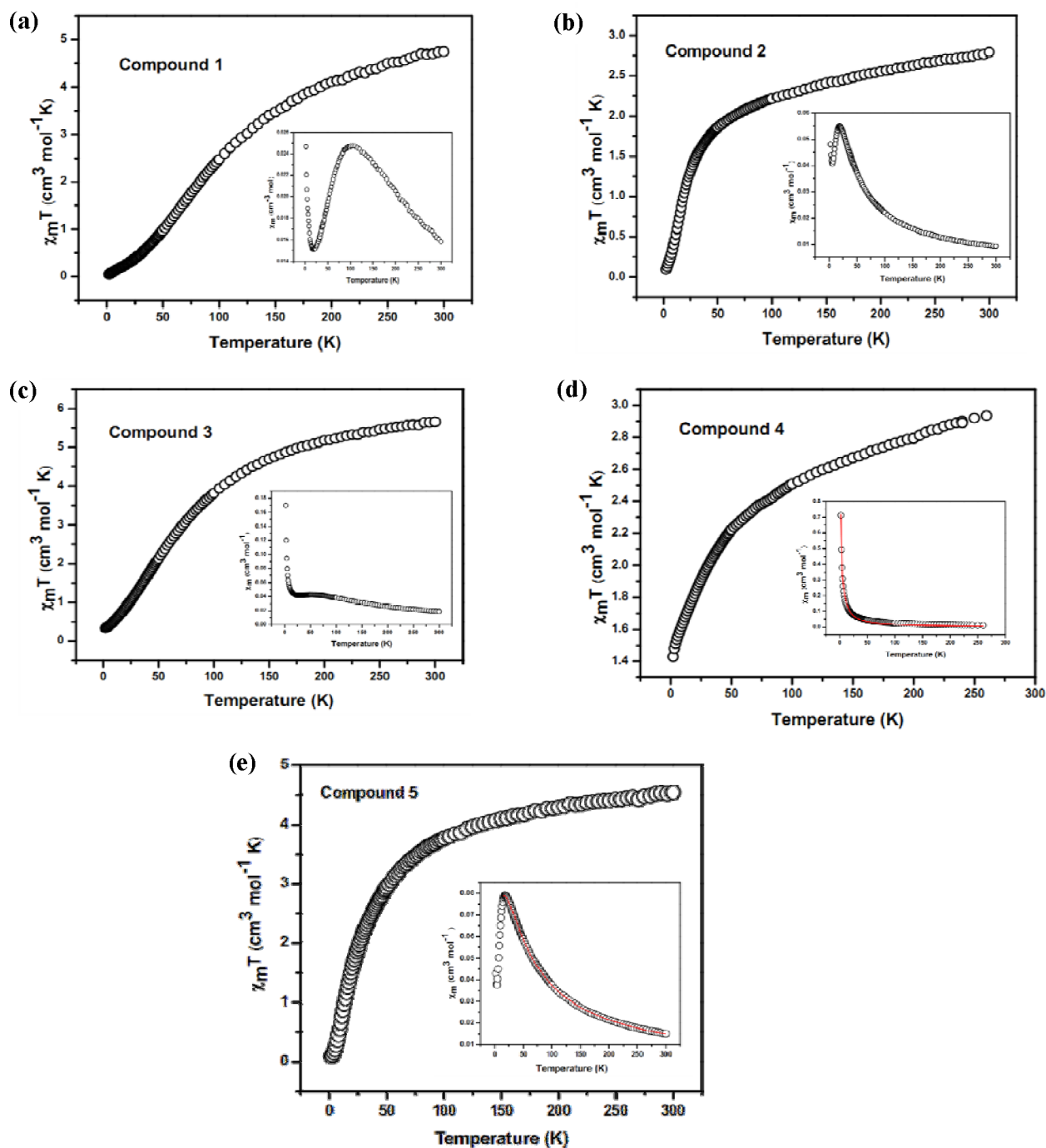
Figure 10. Plots of $\chi_M T$ vs T and χ_M vs T (inset) for the compounds **1–5** in the temperature range of 2–300 K: (a) compound **1**, (b) compound **2**, (c) compound **3**, (d) compound **4**, and (e) compound **5**. The red line indicates the fitting using theoretical model (see text).

mol^{-1} for two Co(II) ions indicating the unquenched orbital contribution from $^4T_{1g}$ ground state of the Co(II) octahedral ion. By lowering the temperature, the $\chi_M T$ value continuously decreases up to 0.34 cm^3 K mol^{-1} at 2 K. A small hump is observed in the χ_M vs T plot in the region of 50–110 K. The 1/χ_M vs T plot follows the Curie–Weiss law with a large negative Weiss constant of $\Theta = -90.4$ K. The large negative value of Θ indicates the strong antiferromagnetic coupling between the adjacent Co^{2+} ions through the carboxylate bridges. The Co–Co distance in the paddle-wheel of compound **3** is 2.844 Å.

Compound 4. The plots of both χ_M vs T and $\chi_M T$ vs T for compound **4** are shown in Figure 10d. Room temperature

$\chi_M T_{300}$ value of 2.93 cm^3 K mol^{-1} is higher than the expected value for isolated Co^{II} ions ($\chi_M T = 1.875$ cm^3 K mol^{-1} for a $S = 3/2$ ion). As the temperature is lowered, the $\chi_M T$ decreases smoothly to 1.42 cm^3 K mol^{-1} at 2 K. 1/χ_M vs T plot follows the Curie–Weiss law at the high temperature with negative Weiss constant $\theta = -29.67$ K. In this compound, the higher value of $\chi_M T$ than the expected spin-only value indicates the orbital contribution of the octahedral Co(II) ion. The observed spin–orbit coupling in compound **4** can be calculated by the expression for $S = 3/2$ systems with dominant zero field splitting effects, D,[25] (eqs 1–4)

$$\chi_{\parallel} = (Ng^2\beta^2 / KT)[A / B] \tag{1}$$

where $A = [1 + 9 \exp(-2D/KT)]$ and $B = [4(1 + \exp(-2D/KT)]$

$$\chi_{\perp} = (Ng^2\beta^2 / KT)[C / D] \tag{2}$$

where $C = [4 + (3KT/D)(1 - \exp(-2D/KT)]$ and $D = [4(1 + \exp(-2D/KT)]$

$$\chi_M' = [(\chi_{\parallel} + \chi_{\perp})/3] \tag{3}$$

$$\chi_M = \chi_M'/\{1 - \chi_M'(2zJ' / Ng^2\beta^2)\} \tag{4}$$

The parameters N, β, and K have their normal meanings. The best fit obtained from 2−300 K with $g = 2.13(2)$, $D = -6.62(1)$ cm^{-1}, and $zJ' = -2.53$ (6) with an agreement factor of 2.4×10^{-4}. The value of D calculated from the above expressions is in the range expected for a pseudo tetrahedral metal center (i.e., $D = -36$ to $+13$ cm^{-1}).[25b]

Compound 5. As shown in Figure 10e, the room temperature (300 K) $\chi_M T$ product amounts to 4.54 cm^3 K mol^{-1}, which is greater than the expected value of 3.75 cm^3 K mol^{-1} for two isolated high-spin Co(II) ions ($g = 2$ and $S = 3/2$). As the temperature is lowered, the $\chi_M T$ value continuously decreases to 3.04 cm^3 K mol^{-1} at 54 K and then sharply decreases up to 2 K reaching a minimum value of 0.085 cm^3 K mol^{-1}. The $1/\chi_M$ vs T plot follows the Curie−Weiss law with negative Weiss constant $\Theta = -33.97$ K. The decrease in $\chi_M T$ value with temperature and negative Weiss constant suggest antiferromagnetic interactions between the two Co(II) ions in the paddle-wheel structure. The magnetic data are fitted assuming that two Co(II) ions bridge by carboxylate ligands form an isolated spin dimer. By introducing interdimer magnetic coupling constant zJ', the magnetic susceptibility data can be fitted from the following equation which is deduced from the spin Hamiltonian.[26]

$$H = -2JS_1 \cdot S$$

where S_1 and S_2 are the spin operators with $S_1 = S_2 = 3/2$.

$$E(S_T) = -JS_T(S_T + 1)$$

$$S_T = 0, 1, 2, 3$$

$$E(S_T) = 0, -J, -3J, -6J$$

$$\chi_M = \chi_M'/\{1 - \chi_M'(2zJ' / Ng^2\beta^2)\}$$

$$\chi_M' = (2Ng^2\beta^2 / KT)[A/B]$$

where $A = [\exp(2J/KT) + 5 \exp(6J/KT) + 14 \exp(12J/KT)]$ and $B = [1 + 3 \exp(2J/KT) + 5 \exp(6J/KT) + 7 \exp(12J/KT)]$.

The parameters N, β, and K have their normal meanings. The best fit of the theoretical equation to the experimental data leads to the $g = 2.29 (3)$ $J = -3.81(2)$ cm^{-1} and $zJ' = -2.80(7)$ with agreement factor of 4.7×10^{-6} (where $R = \Sigma[(\chi_M T)_{exp} - (\chi_M T)_{cal}]^2/\Sigma(\chi_M T)_{exp}^2)$. The nature of the curves and the magnitude of the exchange parameters are consistent with Co-paddle-wheel structures in the literature.[27]

CONCLUSION

Structural chemistry of six Co(II) coordination polymers involving two isomeric long flexible secondary ligands with three different bent carboxylic acids has been discussed. In this study, we have demonstrated the steric hindrance created by the secondary ligand at the metal coordination sphere plays an important role in driving the self-assembly process. When the flexible pyridyl ligands L1 and L2 are used as secondary ligands along with carboxylic acids, the conformation, and position of the ligating atom in the secondary ligand have a substantial role in the formation of diverse architectures in title coordination polymers. Because of the attachment of the bulky group at the second position to the ligating atom in the secondary ligand L1, it creates more crowdedness at the metal coordination sphere in the compounds 1, 3, and 5 and forbids the another bulky ligand into the coordination sphere resulting in the formation of metal carboxylate paddle-wheels with long metal to metal bond. These paddle-wheels along the skeleton of the carboxylate form metal acid layers viz. interpenetrated helical double layers in 1, non-interpenetrated double layers in 2, and single planar layer in 3. The metal acid layers are pillared by the secondary ligand L1 to form layered-pillared architectures in 1, 3, and 5. However, the attachment of bulky group at the third position to the ligating atom in ligand L2 decreases the crowdedness at the metal coordination sphere and allows the other bulky ligands into the coordination sphere thereby forming the diverse architectures in the compounds 2, 4, and 6. When the metal coordination sphere has a tendency to allocate two less crowded secondary ligands L2 then the flexibility in ligand L2 modulates to different conformations, that is, *trans−trans−trans* in 2, *cis−cis−trans* in 3, and *cis−trans−cis* in 4 to meet the coordination requirements at the coordination sphere. The positional isomeric flexible bis(pyridyl) ligands L1 and L2 have also propensity to modulate the conformation of the primary carboxylate ligand pda^{2-} from *trans* conformation in compound 5 to *cis* conformation in compound 6. The conformations of the pyridyl ligands are explained based on the torsion angle measurements. Thermal, electronic, and magnetic properties have also been described. In summary, the present article describes the role of secondary ligand in terms of bulkiness in designing the coordination architectures with potential functionalities.

ASSOCIATED CONTENT

⑤ Supporting Information

Crystallographic data in CIF format, PXRD patterns, $1/\chi_M$ vs T plots, Electonic absorption spectra of the ligands, selected bond distances, and angles in PDF format. This information is available free of charge via the Internet at http://pubs.acs.org.

AUTHOR INFORMATION

Corresponding Author

*E-mail: skdsc@uohyd.ernet.in; samar439@gmail.com. Fax: +91-40-2301-2460. Tel:+91-40-2301-1007.

Notes

The authors declare no competing financial interest.

ACKNOWLEDGMENTS

■ REFERENCES

(1) (a) Halper, S. R.; Do, L.; Stork, J. R.; Cohen, S. M. *J. Am. Chem. Soc.* **2006**, *128*, 15255. (b) Hasegawa, S.; Horike, S.; Matsuda, R.; Furukawa, S.; Mochizuki, K.; Kinoshita, Y.; Kitagawa, S. *J. Am. Chem. Soc.* **2007**, *129*, 2607. (c) Kitagawa, S.; Matsuda, R. *Coord. Chem. Rev.* **2007**, *251*, 2490. (d) Yaghi, O. M.; O'Keeffe, M.; Ockwig, N. W.; Chae, H. K.; Eddaoudi, M.; Kim, J. *Nature* **2003**, *423*, 705. (e) Luo, F.; Zheng, J. M.; Batten, S. R. *Chem. Commun.* **2007**, 3744. (f) Moulton, B.; Zaworotko, M. J. *Chem. Rev.* **2001**, *101*, 1629. (g) Rao, V. K.; Chakrabarti, S.; Natarajan., S. *Inorg. Chem.* **2007**, *46*, 10781.

(2) (a) Qi, Y.; Che, Y. X.; Zheng, J. M. *CrystEngComm* **2008**, *10*, 1137. (b) Henninger, S. K.; Habib, H. A.; Janiak, C. *J. Am. Chem. Soc.* **2009**, *131*, 2776. (c) Ma, L. F.; Wang, L. Y.; Wang, Y. Y.; Du, M.; Wang, J. G. *CrystEngComm* **2009**, *11*, 109. (d) Habib, H. A.; Sanchiz, J.; Janiak, C. *Inorg. Chim. Acta* **2009**, *362*, 2452. (e) Habib, H. A.; Hoffmann, A.; Hoppe, H. A.; Janiak, C. *Dalton Trans.* **2009**, 1742. (f) Habib, H. A.; Sanchiz, J.; Janiak, C. *Dalton Trans.* **2008**, 1734. (g) Zhang, L. P.; Yang, J.; Ma, J. F.; Jia, Z. F.; Xie, Y. P.; Wei, G. H. *CrystEngComm* **2008**, *10*, 1410. (h) Wisser, B.; Lu, Y.; Janiak, C. Z. *Anorg. Allg. Chem.* **2007**, *633*, 1189. (i) Manna, S. C.; Okamoto, K. I.; Zangrando, E.; Chaudhuri, N. R. *CrystEngComm* **2007**, *9*, 199. (j) Chen, Z. F.; Zhang, S. F.; Luo, H. S.; Abrahams, B. F.; Liang, H. *CrystEngComm* **2007**, *9*, 27. (k) Yao, J.; Lu, Z. D.; Li, Y. Z.; Lin, J. G.; Duan, X. Y.; Gao, S.; Meng, Q. J.; Lu, C. S. *CrystEngComm* **2008**, *10*, 1379.

(3) (a) Schaate, A.; Klingelhofer, S.; Behrens, P.; Wiebcke, M. *Cryst. Growth Des.* **2008**, *8*, 3200. (b) Liu, Y.; Qi, Y.; Lv, Y. Y.; Che, Y. X.; Zheng, J. M. *Cryst. Growth Des.* **2009**, *9*, 4797. (c) Li, Z. X.; Hu, T. L.; Ma, H.; Zeng, Y. F.; Li, C. J.; Tong, M. L.; Bu, X. H. *Cryst. Growth Des.* **2010**, *10*, 1138. (d) Yang, J.; Ma, J. F.; Battern, S. R.; Su, Z. M. *Chem. Commun.* **2008**, 2223. (e) Pachfule, P.; Dey, C.; Panda, T.; Banarjee, R. *CrystEngComm* **2010**, *12*, 1600.

(4) (a) Chen, B.; Ockwig, N. W.; Millward, A. R.; Contreras, D. S.; Yaghi, O. M. *Angew. Chem., Int. Ed.* **2005**, *44*, 4745. (b) Cho, S.-H.; Ma, B.; Nguyen, S. T.; Hupp, J. T.; Albrecht-Schmitt, T. E. *Chem. Commun.* **2006**, 2563. (c) Chen, B.; Ma, S.; Zapata, F.; Lobkovsky, E. B.; Yang, Y. *Inorg. Chem.* **2006**, *45*, 5718. (d) Chen, B.; Fronczek, F. R.; Courtney, B. H.; Zapata, F. *Cryst. Growth Des.* **2006**, *6*, 825. (e) Chen, B.; Ma, S.; Zapata, F.; Fronczek, F. R.; Lobkovsky, E. B.; Zhou, H.-C. *Inorg. Chem.* **2007**, *46*, 1233. (f) Pichon, A.; Fierro, C. M.; Nieuwenhuyzen, M.; James, S. L. *CrystEngComm* **2007**, *9*, 449. (g) Li, J. Y.; Olson, D. H.; Pan, L.; Emge, T. J.; Li, J. *Adv. Funct. Mater.* **2007**, *17*, 1255. (h) Chen, B.; Ma, S.; Hurtado, E. J.; Lobkovsky, E. B.; Zhou, H.-C. *Inorg. Chem.* **2007**, *46*, 8490. (i) Tanaka, D.; Horike, S.; Kitagawa, S.; Ohba, M.; Hasegawa, M.; Ozawa, Y.; Toriumi, K. *Chem. Commun.* **2007**, 3142. (j) Choi, E.-Y.; Park, K.; Yang, C.-M.; Kim, H.; Son, J.-H.; Lee, S. W.; Lee, Y. H.; Min, D.; Kwon, Y.-U. *Chem.—Eur. J.* **2004**, *10*, 5535.

(5) (a) Blake, A. J.; Champness, N. R.; Chung, S. S. M.; Li, W. S.; Schröder, M. *Chem. Commun.* **1997**, 1005. (b) Maekawa, M.; Konaka, H.; Suenaga, Y.; Sowa, T. K.; Munakata, M. *Dalton Trans.* **2000**, 4160. (c) Wu, H. C.; Thanasekaran, P.; Tsai, C. H.; Wu, J. Y.; Huang, S. M.; Wen, Y. S.; Lu, K. L. *Inorg. Chem.* **2006**, *45*, 295. (d) Cho, B. Y.; Min, D.; Lee, S. W. *Cryst. Growth Des.* **2006**, *6*, 342. (e) Gao, E. Q.; Cheng, A. L.; Xu, Y. X.; Yan, C. H.; He, M. Y. *Cryst. Growth Des.* **2005**, *5*, 1005. (f) Halder, G. J.; Neville, S. M.; Kepert, C. J. *CrystEngComm* **2005**, *7*, 266. (g) Dybtsev, D. N.; Chun, H.; Kim, K. *Chem. Commun.* **2004**, 1594. (h) Liu, G. F.; Zhang, W. H.; Chen, Y.; Liu, D.; Lang, J. P. *Inorg. Chem. Commun.* **2007**, *10*, 1049. (i) Tripuramallu, B. K.; Kishore, R.; Das, S. K. *Inorg. Chim. Acta* **2011**, *368*, 132. (j) Abrahams,

B. F.; Batten, S. R.; Hamit, H.; Hoskins, B. F.; Robson, R. *Angew. Chem., Int. Ed. Engl.* **1996**, *35*, 1690.

(6) Blake, A. J.; Brooks, N. R.; Champness, N. R.; Crew, M.; Deveson, A.; Fenske, D.; Gregory, D. H.; Hanton, L. R.; Hubberstey, P.; Schröder, M. *Chem. Commun.* **2001**, 1432.

(7) (a) Li, G.; Lu, J.; Li, X.; Yang, H.; Cao, R. *CrystEngComm* **2010**, *12*, 3780. (b) Liu, T. F.; Lu, J.; Lin, X.; Cao, R. *Chem. Commun.* **2010**, *46*, 8439. (c) Li, X.; Weng, X.; Tang, R.; Lin, Y.; Ke, Z.; Zhou, W.; Cao, R. *Cryst. Growth Des.* **2010**, *10*, 3228. (d) Liu, T. F.; Lu, J.; Cao, R. *CrystEngComm* **2010**, *12*, 660. (e) Tripuramallu, B. K.; Kishore, R.; Das, S. K. *Polyhedron* **2010**, *29*, 2985.

(8) (a) Tripuramallu, B. K.; Manna, P.; Reddy, S. N.; Das, S. K. *Cryst. Growth Des.* **2012**, *12*, 777. (b) Bolligarla, R.; Das, S. K. *CrystEngComm* **2010**, 3409.

(9) (a) Wu, Y.-P.; Li, D.-S.; Fu, F.; Dong, W.-W.; Zhao, J.; Zou, K.; Wang, Y.-Y. *Cryst. Growth Des.* **2011**, *11*, 3850. (b) Qin, L.; Hu, J.-S.; Li, Y.-Z.; Zheng, H.-G. *Cryst. Growth Des.* **2012**, *12*, 403.

(10) (a) Tang, E.; Dai, Y.-M.; Lin, S. *Acta Crystallogr. Sect. E: Struct. Rep. Online* **2004**, *60*, m1095. (b) Chen, Y.; Li, H.-X.; Liu, D.; Liu, L.-L.; Li, N.-Y.; Ye, H.-Y.; Zhang, Y.; Lang, J.-P. *Cryst. Growth Des.* **2008**, *8*, 3810. (c) Hu, S.; Zhou, A.-J.; Zhang, Y.-H.; Ding, S.; Tong, M.-L. *Cryst. Growth Des.* **2006**, *6*, 2543. (d) Niu, Y.; Song, Y.; Zhang, N.; Hou, H.; Che, D.; Fan, Y.; Zhu, Y.; Duan, C. *Eur. J. Inorg. Chem.* **2006**, 2259. (e) Hu, S.; Tong, M. L. *Dalton Trans.* **2005**, 1165. (f) Wang, X.-Q.; Cheng, J.-K.; Wen, Y. -H.; Zhang, J.; Li, Z. -J.; Yao, Y. G. *Inorg. Chem. Commun.* **2005**, *8*, 897.

(11) (a) Batsanov, A. S.; Begley, M. J.; Hubberstey, P.; Stroud, J. *Dalton Trans.* **1996**, 1947. (b) Blake, A. J.; Brooks, N. R.; Champness, N. R.; Crew, M.; Deveson, A.; Fenske, D.; Gregory, D. H.; Hanton, L. R.; Hubberstey, P.; Schröder, M. *Chem. Commun.* **2001**, 1432. (c) Peng, R.; Wu, T.; Li, D. *CrystEngComm* **2005**, *7*, 595. (d) Wang, J.; Zheng, S.-L.; Hu, S.; Zhang, Y.-H.; Tong, M.-L. *Inorg. Chem.* **2007**, *46*, 795. (e) Zhang, J.; Cheng, J.-K.; Qin, Y.-Y.; Li, Z.-J.; Yao, Y.-G. *Inorg. Chem. Commun.* **2008**, *11*, 164. (f) Hao, Z.-M.; Fang, R.-Q.; Wu, H.-S.; Zhang, X.-M. *Inorg. Chem.* **2008**, *47*, 8197.

(12) Zhou, X. H.; Wu, T.; Li, D. *Inorg. Chim. Acta* **2006**, *359*, 1442.

(13) (a) Yue, N. L. S.; Jennings, M. C.; Puddephatt, R. J. *Inorg. Chem.* **2005**, *44*, 1125. (b) Burchell, T. J.; Puddephatt, R. J. *Inorg. Chem.* **2006**, *45*, 650. (c) Sagué, J. L.; Fromm, K. M. *Cryst. Growth Des.* **2006**, *6*, 1566. (d) Burchell, T. J.; Eisler, D. J.; Puddephatt, R. J. *Chem. Commun.* **2004**, 944. (e) Muthu, S.; Yip, J. H. K.; Vittal, J. J. *Dalton Trans.* **2002**, 4561. (f) Muthu, S.; Yip, J. H. K.; Vittal, J. J. *Dalton Trans.* **2001**, 3577. (g) Hsu, Y. F.; Chen, J. D. *Eur. J. Inorg. Chem.* **2004**, 1488. (h) Hu, H. L.; Yeh, C. W.; Chen, J. D. *Eur. J. Inorg. Chem.* **2004**, 4696.

(14) (a) Habermehl, N. C.; Angus, P. M.; Kilah, N. L.; Norén, L.; Rae, A. D.; Willis, A. C.; Wild, S. B. *Inorg. Chem.* **2006**, *45*, 1445. (b) Patra, G. K.; Goldberg, I. *Cryst. Growth Des.* **2003**, *3*, 321. (c) Bowyer, P. K.; Porter, K. A.; Rae, A. D.; Willis, A. C.; Wild, S. B. *Chem. Commun.* **1998**, 1153. (d) Patra, G. K.; Goldberg, I. *Dalton Trans.* **2002**, 1051. (e) Sarkar, M.; Biradha, K. *CrystEngComm* **2004**, *6*, 310. (f) Fielden, J.; Long, D. L.; Evans, C.; Cronin, L. *Eur. J. Inorg. Chem.* **2006**, 3930.

(15) (a) Deng, Z. P.; Qi, H. L.; Huo, L. H.; Ng, S. W.; Zhaoa., H.; Gao., S. *Dalton Trans.* **2010**, *39*, 10038. (b) Deng, Z. P.; Zhu, L. N.; Gao, S.; Huo, L. H.; Ng, S. W. *Cryst. Growth Des.* **2008**, *8*, 3277. (c) Deng, Z. P.; Huo, L. H.; Qi, H. L.; Zhu, L. N.; Zhao, H.; Gao, S. *CrystEngComm* **2011**, *13*, 4218. (d) Deng, Z. P.; Huo, L. H.; Qi, H. L.; Zhao, H.; Gao, S. *Inorg. Chem. Commun.* **2011**, *14*, 64.

(16) (a) Zhu, L. N.; Gao, S.; Huo, L. H. *Acta Crystallogr., Sect. E: Struct. Rep. Online* **2007**, *E63*, o4459. (b) Zou, R. Y.; Xu, F. B.; Li, Q. S.; Song, H. B.; Lv, H.; Zhang, Z. Z. *Acta Crystallogr., Sect. E: Struct. Rep. Online* **2003**, *E59*, o1312.

(17) (a) *SAINT: Software for the CCD Detector System*; Bruker Analytical X-ray Systems, Inc.: Madison, WI, 1998. (b) *SADABS: Program for Absorption Correction*; Sheldrick, G. M. University of Gottingen: Gottingen, Germany, 1997. (c) *SHELXS-97: Program for Structure Solution*; Sheldrick, G. M. University of Gottingen: Gottingen, Germany, 1997. (d) *SHELXL-97: Program for Crystal Structure Analysis*; Sheldrick, G. M. University of Gottingen:

Gottingen, Germany, 1997. (e) Blatov, V. A.; Shevchenko, A. P.; Serezhkin, V. N. J. *Appl.Crystallogr.* **2000**, *33*, 1193. TOPOS software is available for download at http://www.topos.ssu.samara.ru.

(18) (a) Han, L.; Zhao, Y.; Zhao, W. N.; Li, X.; Liang, Y. X. *Cryst. Growth Des.* **2009**, *9*, 660. (b) Pachfule, P.; Dey, C.; Panda, T.; Banarjee, R. *CrystEngComm* **2010**, *12*, 1600. (c) Ji, C. C.; Qin, L.; Li, Y. Z.; Guo, Z. J.; Zheng, H. G. *Cryst. Growth Des.* **2011**, *11*, 480.

(19) (a) Sun, C. Y.; Zheng, X. J.; Gao, S.; Li, L. C.; Jin, L. P. *Eur. J. Inorg. Chem.* **2005**, 4150. (b) Tao, J.; Shi, J. X.; Tong, M. L.; Zhang, X. X.; Chen, X. M. *Inorg. Chem.* **2001**, *40*, 6328. (c) Chen, X. M.; Liu, G. F. *Chem.—Eur. J.* **2002**, *8*, 4811.

(20) (a) Liu, Y.; Qi, Y.; Lv, Y. Y.; Che, Y. X.; Zheng, J. M. *Cryst. Growth Des.* **2009**, *9*, 4797. (b) Batten, S. R.; Robson, R. *Angew. Chem., Int. Ed.* **1998**, *37*, 1460. (c) Batten, S. R. *CrystEngComm* **2001**, *3*, 67.

(21) (a) Li, X.; Weng, X.; Tang, R.; Lin, Y.; Ke, Z.; Zhou, W.; Cao, R. *Cryst. Growth Des.* **2010**, *10*, 3229. (b) Blake, K. M.; Johnston, L. L.; Nettleman, J. K.; Supkowskib, R. M.; LaDuca, R. L. *CrystEngComm* **2010**, *12*, 1927. (c) Chen, S. S.; Bai, Z. S.; Fan, J.; Lv, G. C.; Su, Z.; Chena, M. S.; Sun, W. Y. *CrystEngComm* **2010**, *12*, 3091. (d) Blake, K. M.; Banisafar, A.; LaDuca, R. L. *Inorg. Chim. Acta* **2011**, *373*, 201.

(22) Liu, T.; Lu, J.; Shi, L.; Guo, Z.; Cao, R. *CrystEngComm* **2009**, *11*, 583.

(23) Li, R.-Y.; Wang, X.-Y.; Liu, T.; Xu, H.-B.; Zhao, F.; Wang, Z.-M.; Gao, S. *Inorg. Chem.* **2008**, *47*, 8134.

(24) Chen, M.; Chen, S.-S.; Okamura, T.; Su, Z.; Chen, M.-S.; Zhao, Y.; Sun, W.-Y.; Ueyama, N. *Cryst. Growth Des.* **2011**, *11*, 1901.

(25) (a) Marshall, S. R.; Rheingold, A. L.; Dawe, L. N.; Shum, W. W.; Kitamura, C.; Miller, J. S. *Inorg. Chem.* **2002**, *41*, 3599. (b) Makinen, M. W.; Kuo, L. C.; Yim, M. B.; Wells, G. B.; Fukuyama, J. M.; Kim, J. E. *J. Am. Chem. Soc.* **1985**, *107*, 5245.

(26) Kahn, O. *Molecular Magnetism*; VCH Publishers: NewYork, 1993.

(27) Qin, L.; Hu, J.-S.; Huang, L.-F.; Li, Y.-Z.; Guo, Z.-J.; Zheng, H.-G. *Cryst. Growth Des.* **2010**, *10*, 4176.